Frequency spectra for admittances and voltage transfers measured on a three-phase power transformer

Research Report
ISSN 0167-9708
Coden: TEUEDE

Eindhoven
University of Technology
Netherlands

Faculty of Electrical Engineering

Frequency Spectra for Admittances and Voltage Transfers Measured on a Three-Phase Power Transformer

by

M.H.J. Bollen and P.T.M. Vaessen

EUT Report 87-E-181
ISBN 90-6144-181-1
October 1987

Eindhoven University of Technology Research Reports

EINDHOVEN UNIVERSITY OF TECHNOLOGY

Faculty of Electrical Engineering
Eindhoven The Netherlands

ISSN 0167- 9708 Coden: TEUEDE

FREQUENCY SPECTRA FOR ADMITTANCE AND VOLTAGE TRANSFERS MEASURED ON A THREE-PHASE POWER TRANSFORMER

by

M.H.J. Bollen

and

P.T.M. Vaessen

EUT Report 87-E-181
ISBN 90-6144-181-1

Eindhoven
October 1987

CIP-GEGEVENS KONINKLIJKE BIBLIOTHEEK, DEN HAAG

Bollen, M.H.J.

Frequency spectra for admittance and voltage transfers measured on a three-phase power transformer / by M.H.J. Bollen en P.T.M. Vaessen. - Eindhoven: University of Technology, Faculty of Electrical Engineering. - Fig. - (EUT report, ISSN 0167-9708; 87-E-181)
Met lit. opg., reg.
ISBN 90-6144-181-1
SISO 661.75 UDC 621.314.2.015.3 NUGI 832
Trefw.: vermogenstransformatoren / elektrische overgangsverschijnselen.

Abstract

A large number of frequency spectra for admittance and voltage transfer has been measured. The measurements have been carried out on a 25 MVA 150/11 kV transformer. Recorded input and output pulses have been processed with the aid of an FFT algorithm to give admittances and voltage transfers. The results are reliable between 1 kHz and some hundreds of kHz. Below 1 kHz additional measurements have been carried out with a sweep generator and with stationary frequencies. The spectra show large scale phenomena with superimposed maxima and minima probably caused by part-winding resonances. A simple model, consisting of lumped capacitances and inductances is given to reproduce the large scale behaviour.

Bollen, M.H.J. and P.T.M. Vaessen
FREQUENCY SPECTRA FOR ADMITTANCE AND VOLTAGE TRANSFERS MEASURED ON A THREE-PHASE POWER TRANSFORMER.
Faculty of Electrical Engineering, Eindhoven University of Technology, 1987.
EUT Report 87-E-181

Addresses of the authors:

ir. M.H.J. Bollen,
Division of Electrical Energy Systems,
Faculty of Electrical Engineering,
Eindhoven University of Technology,
P.O. Box 513,
5600 MB EINDHOVEN,
The Netherlands

ir. P.T.M. Vaessen,
Research and Development Division,
N.V. KEMA,
Utrechtseweg 310,
6812 AR ARNHEM,
The Netherlands

ACKNOWLEDGEMENT

Thanks are due to Prof.dr.ir. W.M.C. van den Heuvel, Ir. W.F.J. Kersten, Ing. G.A.P. Jacobs and Prof.ir. M. Antal of the Eindhoven University of Technology and to Ir. J.A.A.N. Hooijmans of N.V. KEMA, Arnhem, for their assistance during the measurements and during the realization of this report.

Contents

List of figures

33. Transfer h.v.S to h.v.T divided by the transfer to l.v.T; absolute value.
34. Transfer h.v.S to h.v.T divided by the transfer to l.v.T; argument.
35. No-load l.v.S; absolute value.
36. No-load l.v.S; argument.
37. Short-circuit l.v.S; absolute value.
38. Short-circuit l.v.S; argument.
39. Short-circuit l.v.S; Resistance and inductance for R-L-series-connection.
40. Short-circuit l.v.S; Inductance for R-L-series connection parallel to capacitor.
41. Short-circuit l.v.S; Resistance for R-L-series connection parallel to capacitor.
42. Transfer l.v.S to h.v.S; absolute value.
43. Transfer l.v.S to h.v.S; argument.
44. Transfer l.v.S to l.v.T; absolute value.
45. Transfer l.v.S to l.v.T; argument.
46. Transfer l.v.S to h.v.T; absolute value.
47. Transfer l.v.S to h.v.T divided by the transfer to l.v.T; absolute value.
48. No-load h.v.T; absolute value.
49. No-load h.v.T; argument.
50. No-load h.v.T; absolute value measured with sweep generator.
51. Short-circuit h.v.T; absolute value.
52. Short-circuit h.v.T; argument.
53. Short-circuit h.v.T compared with h.v.S.
54. Transfer h.v.T to l.v.T; absolute value.
55. Transfer h.v.T to l.v.T; argument.
56. Transfer h.v.R to h.v.S; absolute value.
57. Transfer h.v.R to h.v.S; argument.
58. Transfer h.v.R to h.v.S; polar diagram.
59. Transfer h.v.R to l.v.S; absolute value.
60. Transfer h.v.R to h.v.T; absolute value.
61. Transfer h.v.R to l.v.T; absolute value.
62. Transfer h.v.R to h.v.T; polar diagram.
63. Transfer h.v.R to h.v.T and to h.v.S; measured at stationary frequencies.
64. No-load l.v.T; absolute value.
65. No-load l.v.T; argument.
66. Transfer l.v.T to h.v.T; absolute value.
67. Transfer l.v.T to h.v.T; argument.

1. Introduction

Knowledge of the high frequency behaviour of transformers is indispensable for the calculation of transients and overvoltages that can occur in networks which contain transformers. It is also important in the field of transformer protection and can be used as a diagnostic tool since mechanical changes and defects are reflected in the high frequency behaviour of transformers (Dick, Erven, 1978). Finally applications for transformer modelling in electromagnetic transient programs are known (Vaessen, 1987).

In this report results from high frequency admittance and transfer measurements of a three phase 25 MVA transformer are given. They can be used as a starting point for the applications mentioned above.

The method used for the measurements is outlined in section 2, it is based upon the use of the digital recorded time responses from impulse testing. Section 3 is a presentation of measured frequency spectra together with some brief explanation. The development of simple transformer models which describe some of the behaviour are dealt with in section 4. Finally some conclusions are drawn and suggestions for future work are given.

The authors suppose that the measurements presented in this report can be of great interest to others as well. They are willing to give their data to anyone working on transformer modelling for scientific purposes.

2.Measurements.

There are several ways to measure the transfer and admittance functions of transformers. The method used to obtain the results presented in this report is based upon the use of the recorded time responses from impulse testing. An impulse voltage has been applied to a transformer terminal and the required time responses have been recorded with the aid of a digitizer. The digital recorded time functions have been Fourier transformed to obtain the frequency spectra and from these the desired transfer and admittance functions have been calculated.

2.1 Experimental set-up.

The measurements have been done on a 150/11 kV 25 MVA transformer at KEMA-laboratories, Arnhem, Netherlands. The top view of the transformer with winding connections is given in figure 1. More information about the transformer can be found in appendix A. During normal practice r,s and t are connected, to y,z and x respectively, thus making a Yd transformer. During the measurements presented in this report N,x,y, and z have been connected with the tank of the transformer giving a YNyn transformer with a turns ratio of 7.9.

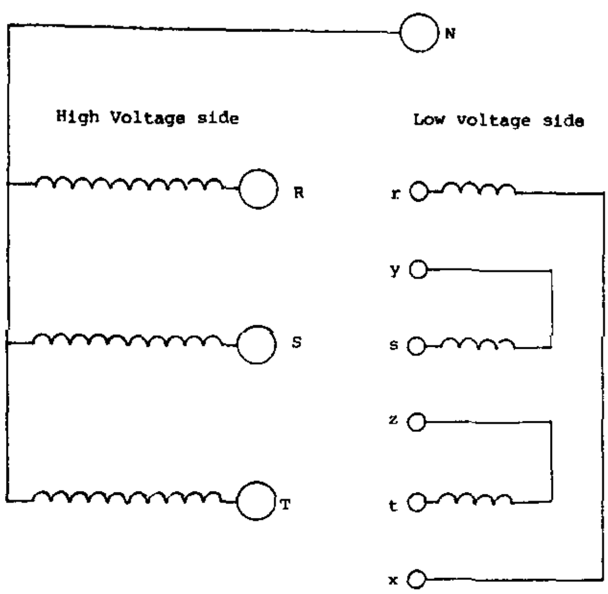

Figure 1: Top view of the transformer with winding connections.

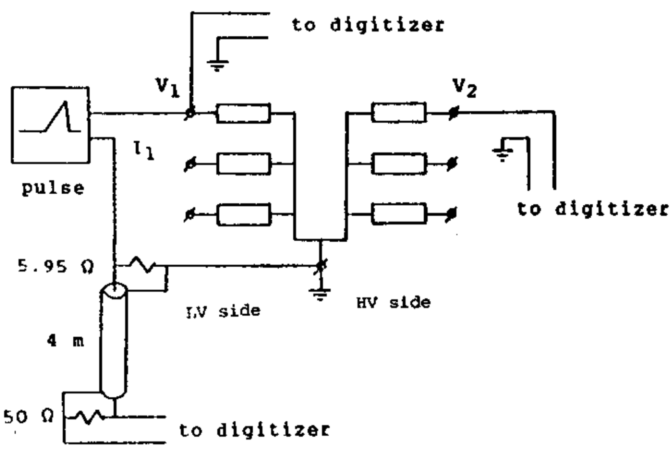

*Figure 2: **Experimental set-up***

Figure 2 shows the experimental set-up. A 3.6/18 µs (IEC 60-2) impulse voltage with a crest value of 250 V (adjustable) has been used as the input signal. The applied voltage as well as the transfered voltage have been measured with a high impedance voltage probe in order to avoid loading the transformer. Current has been measured with a coaxial shunt of 5.95 Ohm parallel to a 4 meter coaxial cable, characteristicly terminated.

The signals have been recorded on a two channel 10 bit digitizer with 2k-words of memory for each channel. A computer has been used for automated measurements. The recordings are stored on floppy-disk. The entire set-up has been powered by a 3 kVA isolation transformer. The tank of the transformer to be measured has been connected to both winding star points and has been used as ground reference.

Current measurements with the shunt are reliable as long as the transformer impedance keeps well above 5 Ω. This can be a problem for admittance measurements carried out on the low voltage side of the transformer, which has less impedance than the high voltage side.

The 10 bit A/D converter of the digitizer has a signal-to-noise-ratio of approximately 60 dB caused by the quantisation of the recorded signals. This means that signal components that are too small can not be distinguished from the bit-noise caused by the digitizer. The frequency spectrum of the impulse voltage used remains well above the bit-noise level up to 1 MHz. Given the fact that the main resonances of the transformer lie below 200 kHz a sample frequency of 1 MHz has been chosen for the digitizer. With this choice of the sample frequency aliasing is avoided. The memory size of 2k-words allows for a time registration of 2.048 ms and after computation a frequency spectrum up to 500 kHz with a resolution of 488.3 Hz. The frequency spectra have been calculated using an FFT algoritm.

2.2. Processing of the measurements.

From the recorded signals frequency spectra have been calculated. From these spectra, admittances and transfer functions can be determined. This will be demonstrated by means of an example.

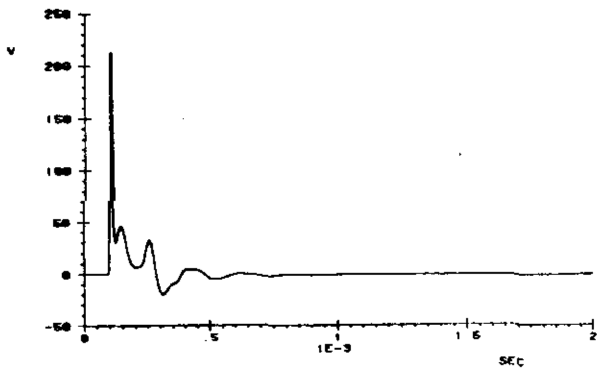

Figure 3: Recorded values of input voltage.

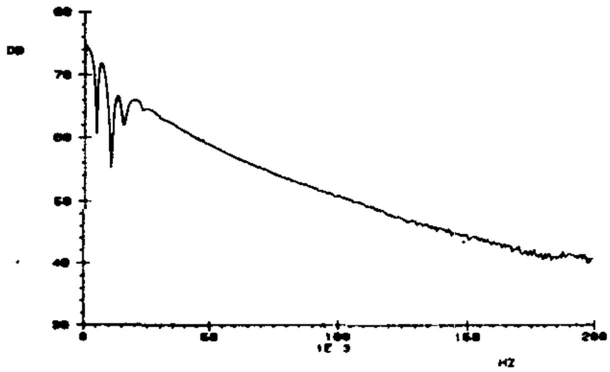

Figure 4: Spectrum of input voltage.

Figure 3 shows the measured input voltage on low-voltage side $V_1(t)$. Figure 4 shows the corresponding frequency spectrum $|V_1(j\omega)|$ (only absolute value). Figure 5 and 6 show measured input current on low-voltage side $I_1(t)$ and frequency spectrum $|I_1(j\omega)|$ respectively. Figure 7 and 8 show this for the transfered voltage V_2.

Frequency spectra have been given up to 200 kHz. The vertical units are dB's (0 dB corresponds to 1 μV/Hz)

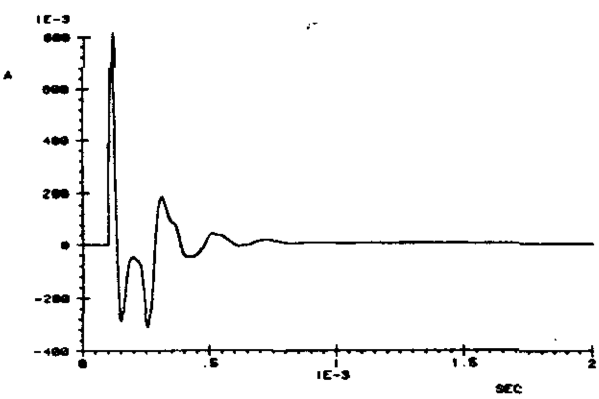

Figure 5: Recorded values of input current.

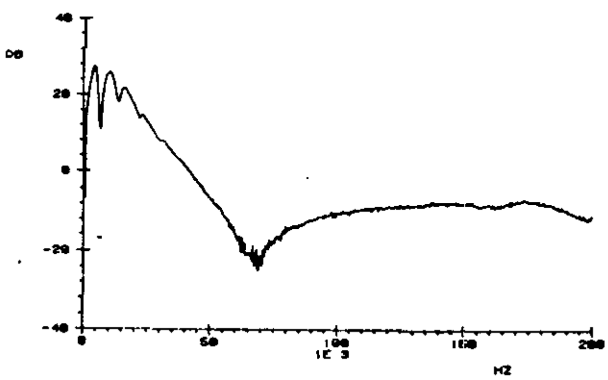

Figure 6: Spectrum of input current.

Notice the deformation of the applied impulse due to the transformer. The bit-noise caused by the digitizer can be seen clearly in the minimum at 65 KHz in the spectrum of the primary current (Figure 6) and above 120 kHz in the spectrum of the transfered voltage (Figure 8). For these parts of the spectra the reliability of the measurements is low. The coherence function (Roth, 1971), an indication for the reliability, produces low values in these regions.

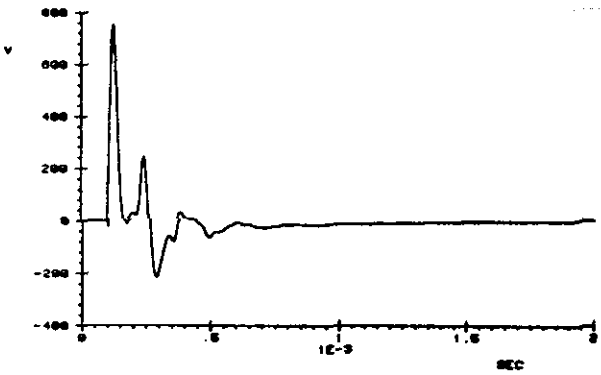

Figure 7: ***Recorded values of transfered voltage.***

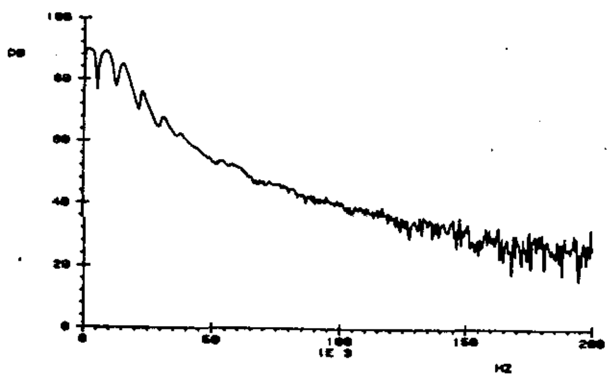

Figure 8: ***Spectrum of transfered voltage.***

The admittance $Y(j\omega)$ and transfer function $H(j\omega)$ can be determined from the calculated frequency spectra by:

$$Y(j\omega) = \frac{I_1(j\omega)}{V_1(j\omega)} \quad \text{and} \quad H(j\omega) = \frac{V_2(j\omega)}{V_1(j\omega)}$$

Figure 9 gives the absolute value of the calculated no-load input admittance on low-voltage side $Y(j\omega)$ on the center leg. Figure 10 gives the corresponding transfer to high-voltage side $H(j\omega)$. 0 dB corresponds to 1 A/V for the admittance and 1 V/V for the transfer spectrum.

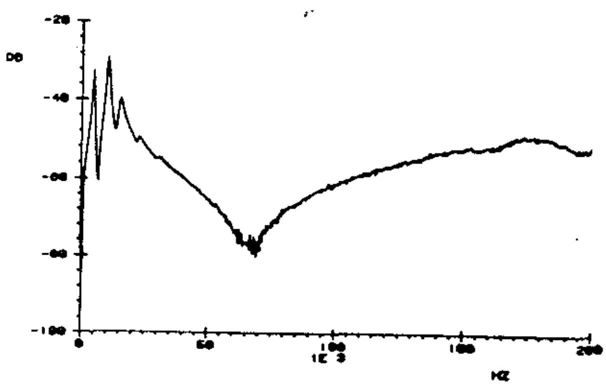

Figure 9: ***Spectrum of admittance***

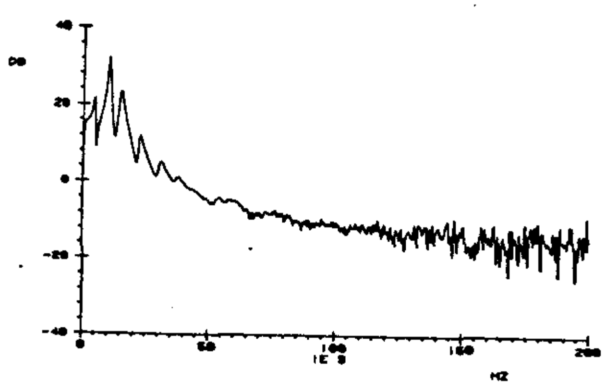

Figure 10: ***Spectrum of transfer function.***

The horizontal resolution of the frequency spectra df has been given by df = SF/MS in which SF is the sample frequency and MS the memory size of the digitizer channel. This resolution can be enhanced by adding zeroes to the registered time signals thus increasing memory size artificially which resuls in a better resolution (smaller df) for the frequency spectrum. The time signals have to be damped out when reaching the end of the time window to prevent errors. If this is not the case, a continuity correction in the time domain has to be made first. Even then oscillatory errors still occur when zero's have been added to these corrected time signals. The height of the oscillations depends on the error which is made at the truncation of the time signals at the end of the time window.

Figure 11 shows the spectrum of the no-load input admittance (like figure 9) while figure 12 shows the calculated spectrum with increased frequency resolution (factor 4) by adding zeroes to the time signals. Figure 13 and 14 show the transfer to the high-voltage side with normal and enhanced resolutions. While the time signals are damped out at the end of the time window no errors occur in the calculated spectra with enhanced resolution. Notice the height of the resonance peaks and the smoothness of the curves for the different situations.

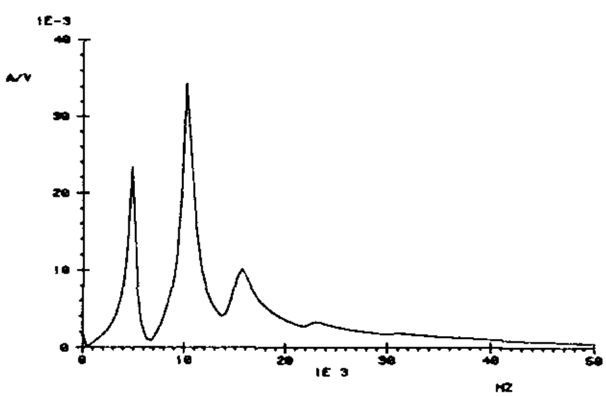

Figure 11: Normal frequency resolution

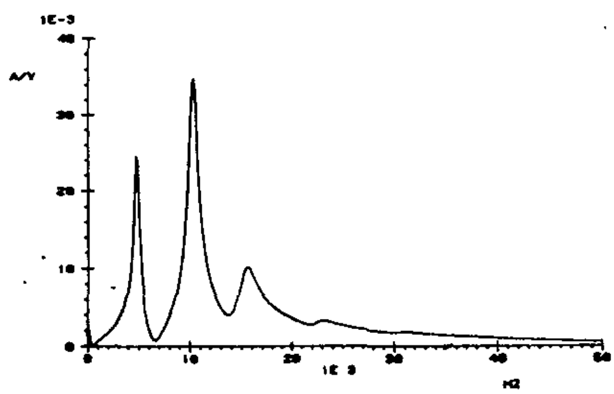

Figure 12: Enhanced resolution.

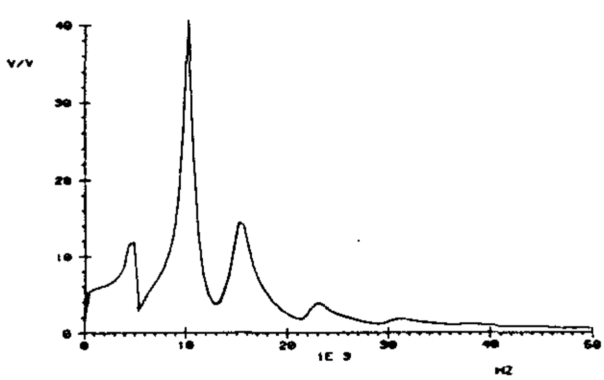

Figure 13: Normal frequency resolution

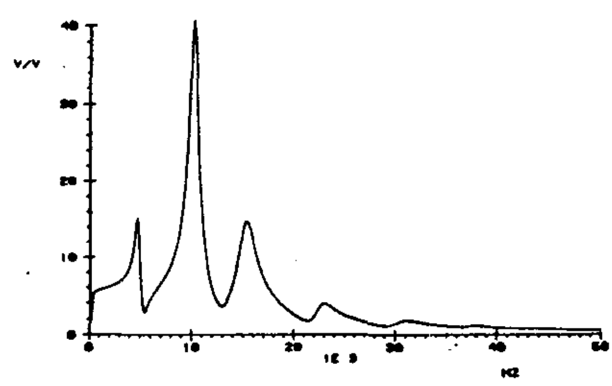

Figure 14: Enhanced resolution.

2.3 Errors introduced.

Two major errors that occur are: too short a time window and too low a sample frequency. They will be discussed here shortly. The second error has been prevented during the measurements, the first one occurs occasionally as can be seen in some of the figures in chapter 3 and in the example shown hereafter. Figure 15 shows a part of the spectrum of the absolute value of the no-load admittance on high-voltage side on the center leg. The corresponding time signals are not damped out at the end of the time window, therefore oscillations occur in the spectrum with enhanced frequency resolution (Figure 16). The effect of the enhancement has been clearly demonstrated at the first resonance frequency of 5 kHz.

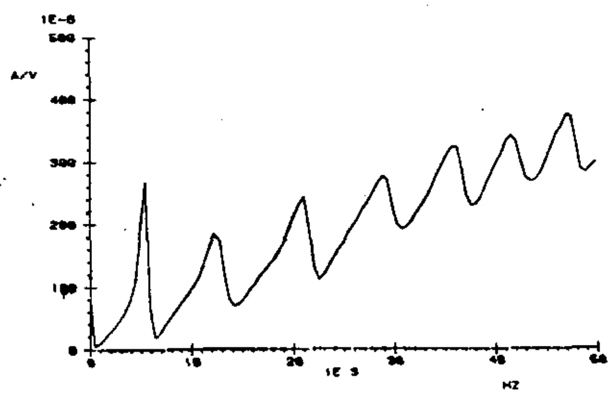

Figure 15: Normal frequency resolution

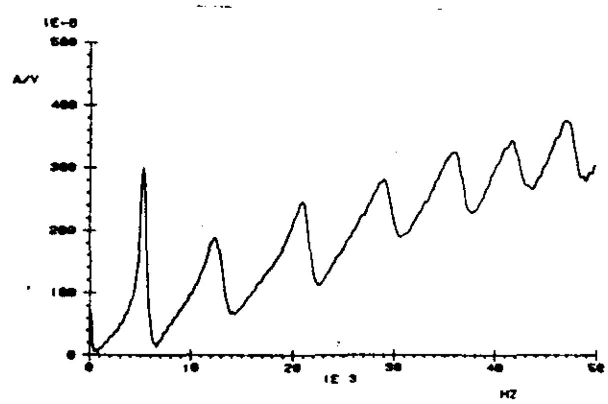

Figure 16: Enhanced resolution.

Aliasing occurs when sampled time signals contain components which have a higher frequency than the Nyquist frequency (half the sample frequency). The higher frequency components have been folded back to lower frequencies as a consequence of the overlap of the partial spectra of the periodic continuated time signal. Once a spectrum has been corrupted with aliasing there is no way to reconstruct the original spectrum. For this reason it is necessary to prevent aliasing.

Three solutions to prevent aliasing are possible. The sample frequency can be raised in order to be shure that the highest occuring signal frequency is less than the Nyquist frequency. With the same memory size the frequency resolution is lowered. A second solution is the use of low-pass filters (anti aliasing filters) at the entrance of the digitizer. Signal components with a frequency above the cut-off frequency of the filter have been attenuated thus reducing the aliasing effect. Frequency resolution has not been affected when using this solution. A practical problem is the difference between the two filters and the extra phase-lag caused by them which leads to errors in the calculated admittances and transfer functions.

For the third solution the input signal has been carefully chosen in order to limit the frequency content above half the sample frequency. So aliasing is prevented, at least substantionally limited without the aid of filters. Even when some resonant frequencies of the transformer occur above the Nyquist frequency aliasing is still limited due to the small energy content of the input signal in this frequency range. This method has been used to obtain the results presented in this report.

3.Results of the measurements

In this chapter a large number of frequency plots is given for all kinds of admittances and voltage transfers. Of most quantities both absolute value and argument are given, sometimes only the absolute value. In some cases additional measurements or the results of some operations are added.
Each paragraph treats one quantity or a few quantities belonging together; both outside legs are always treated in one paragraph, and only one of both plots is given, although both have been measured. The text in each paragraph tells which of both outside legs is shown.
Where possible, an early interpretation of the results is given. In some of those cases references to chapter 4 are unavoidable.

In this chapter some abbreviations will be used. Low-voltage side and high-voltage side will be abbreviated by l.v. and h.v. respectively. Because always admittances are shown and never impedances, the word admittance will be discarded in the text. The three legs will just be denoted R, S and T, S being the center leg. A few examples will be given hereafter. The headings above the paragraphs only use h.v. and l.v. as abbreviations; the text below the figures uses even more abbreviations when necessary to save room.

No-load h.v.S: no-load admittance on the high-voltage side of the center leg (leg S);

short-circuit l.v.T: short-circuit admittance on the low-voltage side of leg T;

transfer h.v.R to l.v.S: voltage transfer from the high-voltage side of leg R to the low-voltage side of the center leg.

3.1. No-load admittance h.v. center leg.

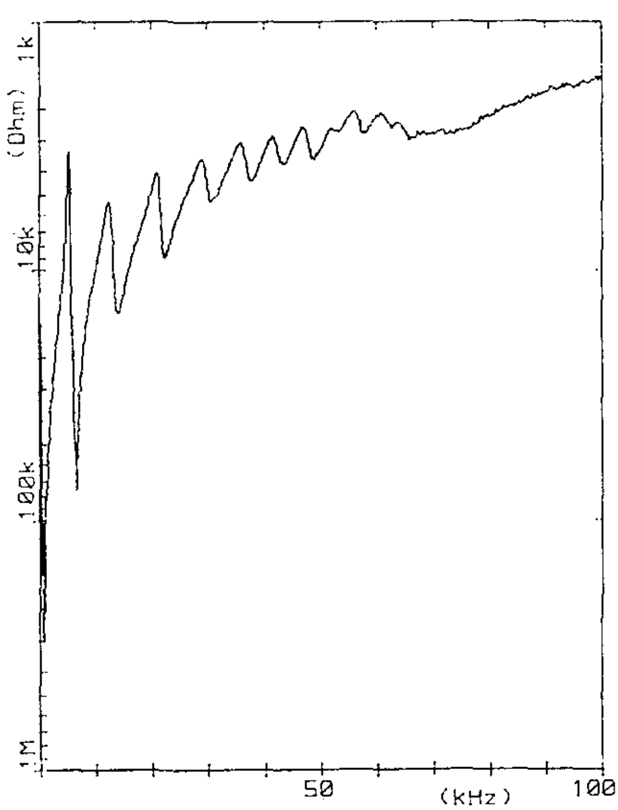

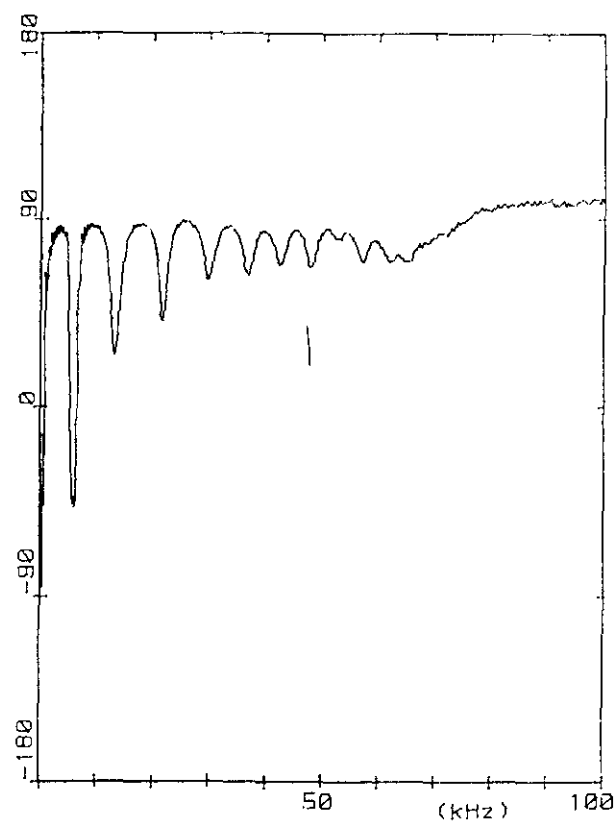

***Figure 17*: No-load h.v.S; absolute value** ***Figure 18*: Argument.**

The no-load h.v.S is shown in figure 17 (absolute value) and figure 18 (argument). One can see the fast decline of the absolute value at low frequencies caused by the large inductance in the no-load situation. The argument of the admittance changes in this frequency range from -90° (inductive) to +90° (capacitive).

For frequencies up to 65 kHz some minima and maxima in the absolute value occur. In the argument sharp peaks are visible. A peak in the argument always coincides with the middle of a declining side in the absolute value as is usual to second-order resonances. At 65 kHz the resonances disappear abruptly. These phenomena are probably caused by resonances of the leakage flux of partial windings, as first described by Wagner [1915]. Above 75 kHz the admittance is that of a capacitor of (770 ± 20) pF. The last quantity has been derived from a log-log-plot of the absolute value up to 1 MHz (not shown here).

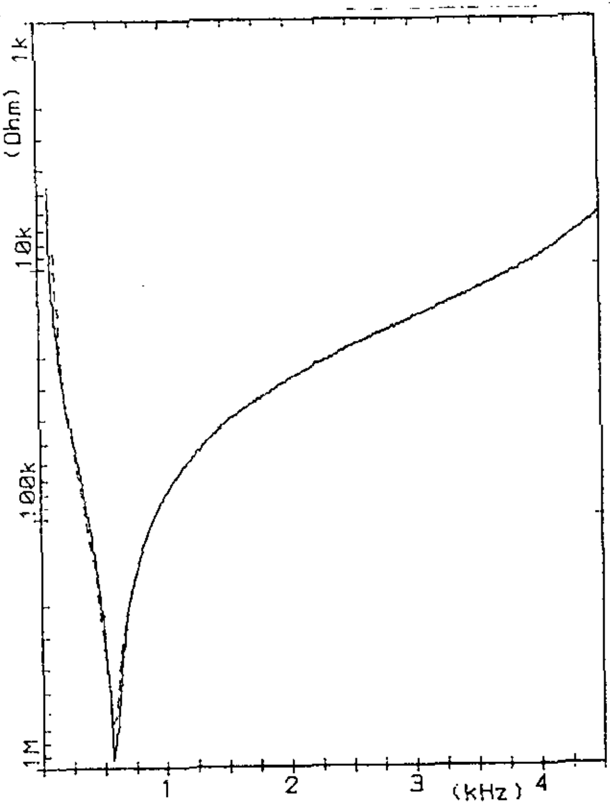

Figure 19: ***No-load h.v.S measured with sweep generator***

The no-load h.v.S also has been measured using a sweep generator with adjustable voltage amplitude. The absolute value of the admittance obtained is given in figure 19 up to 4.5 kHz. Only the absolute value is given because the argument is not easily derived by this method.
The shown curves are for effective values of the voltage on the high-voltage winding of 2V and 100V. The curves for 10V and 50V almost coincide. Although the amplitude does not seem to have much influence on the admittance, it is too early to conclude that this is also the case for higher amplitudes than used here. The high-voltage winding has been designed for a rated voltage of 85 kV, the applied voltage of 100V is much less than 1% of this. At this low voltage the iron is still in the linear part of the magnetisation-characteristic. The use of higher voltages will increase the value of the no-load impedance and so decrease the value of the first resonant frequency. In paragraph 3.11 this phenomena will be outlined further.

3.2. Short-circuit admittance h.v. center leg.

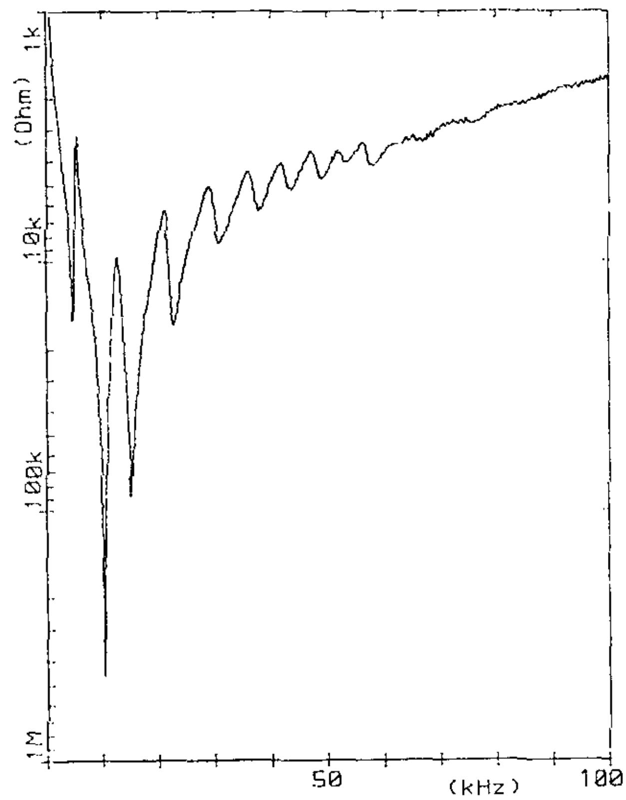

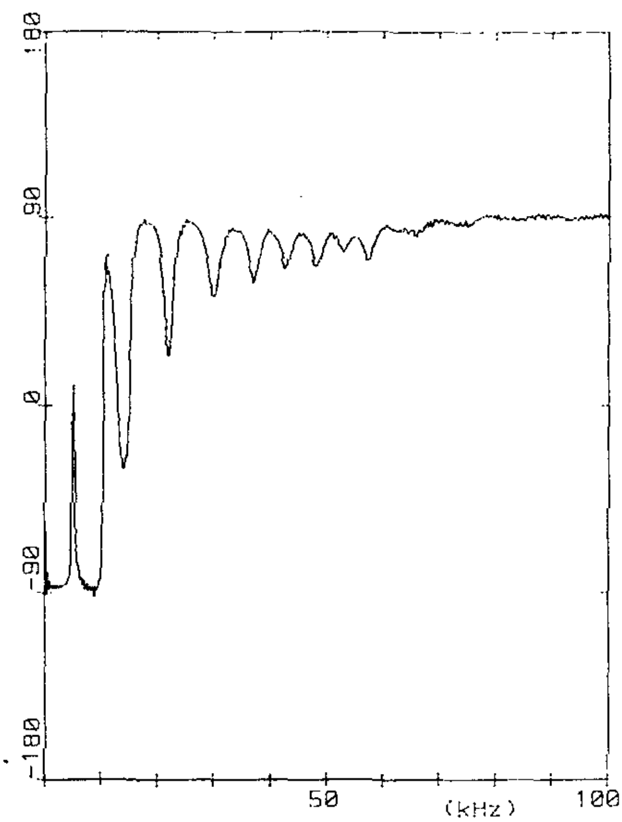

Figure 20: ***Short-circuit h.v.S; abs. val.*** *Figure 21*: ***Argument***

The short-circuit h.v.S is shown in figure 20 (absolute value) and figure 21 (argument). As a first approximation one observes a decrease in admittance up to 10 kHz, and after that an increase. The argument shows a transition from -90° (inductive) to +90° (capacitive).

Further behaviour looks like the behaviour of the no-load h.v.S (Figure 17 and 18). Absolute value maxima are at the same frequency. The same applies to minima above 20 kHz. Above 75 kHz the admittance is that of a capacitor of (850 ± 20) pF.

Freq	*Imped*	*Induct*	*Method*
51 Hz	*63.0 Ω*	*196 mH*	*Stat Freq*
122	*153.5*	*200*	*Pulseresp*
147	*182.1*	*197*	*Stat Freq*
244	*271.9*	*178*	*Pulseresp*
326	*402.1*	*196*	*Stat Freq*
366	*431.5*	*188*	*Pulseresp*
488	*640.1*	*209*	*Pulseresp*

Table 1

The absolute value of the short-circuit admittance also has been measured for some stationary frequencies. The results are given in table 1. From the absolute value an inductance has been derived by the formula

$$L = \frac{|z|}{\omega}$$

This holds as long as the argument of the impedance is close to 90°. The short-circuit inductance is 196 mH according to measurements with stationary frequencies. The average of the four values from pulse measurements is 194 mH, a close agreement. The manufacturer also gives a value of 194 mH (calculated, see appendix A). Because of the finite time window used to measure the pulse, abberations have been introduced in individual frequency points. But by averaging over a few points a high accuracy can be derived. The abberations only exist for low frequencies, they are always detectable as a fast swinging in the frequency plots.

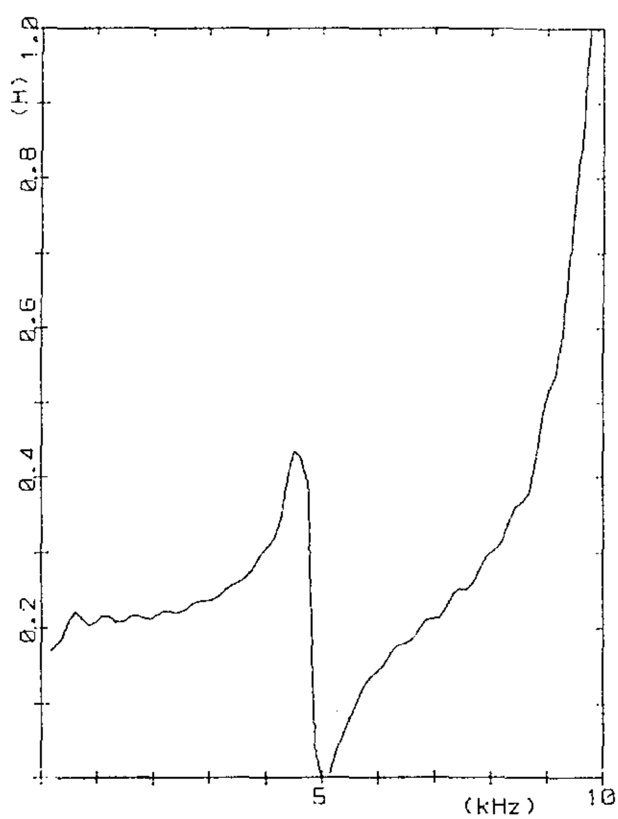

Figure 22 Inductance from short-circuit h.v.S

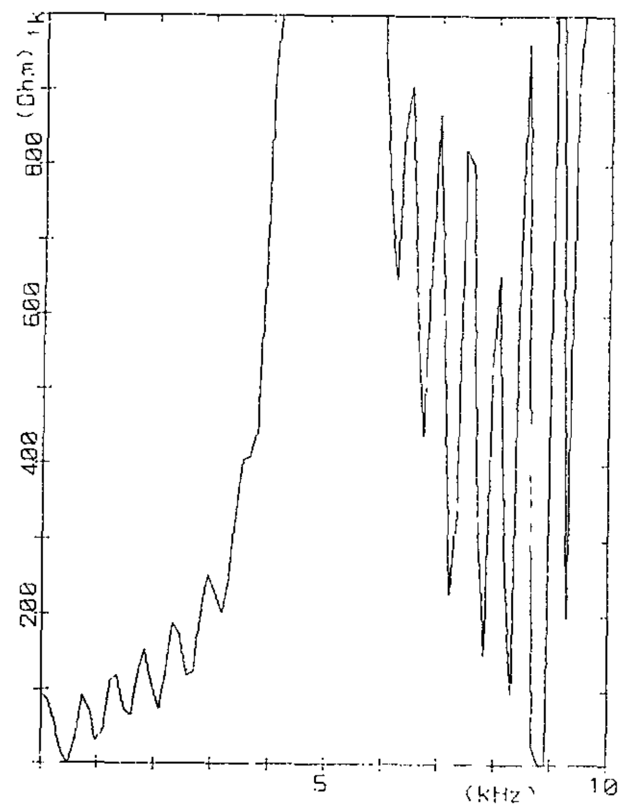

Figure 23: ***Resistance***

Assuming the short-circuit h.v.S can be described as an R-L-series connection, it is possible to derive the resistance R and the inductance L from the real and imaginary part of the admittance. The results for frequencies up to 10 kHz are given in figure 22 (inductance) and figure 23 (resistance). The values are reliable up to about 3 kHz. The assumption of an R-L-series connection is no longer valid for higher frequencies. One can see an inductance fairly constant at 208 mH above 500 Hz. The lower values found below 500 Hz are due to the finite time window used.

At stationairy frequencies it has been shown before that the inductance is constant below 350 Hz. One can conclude that the short-circuit inductance is equal to (200 ± 10) mH up to at least 2 kHz.
The resistance shows an increase from 20 Ω at 100 Hz up to 125 Ω at 2 kHz, caused by eddy currents in the windings (copper loss).

3.3. Transfer from h.v. to l.v. center leg.

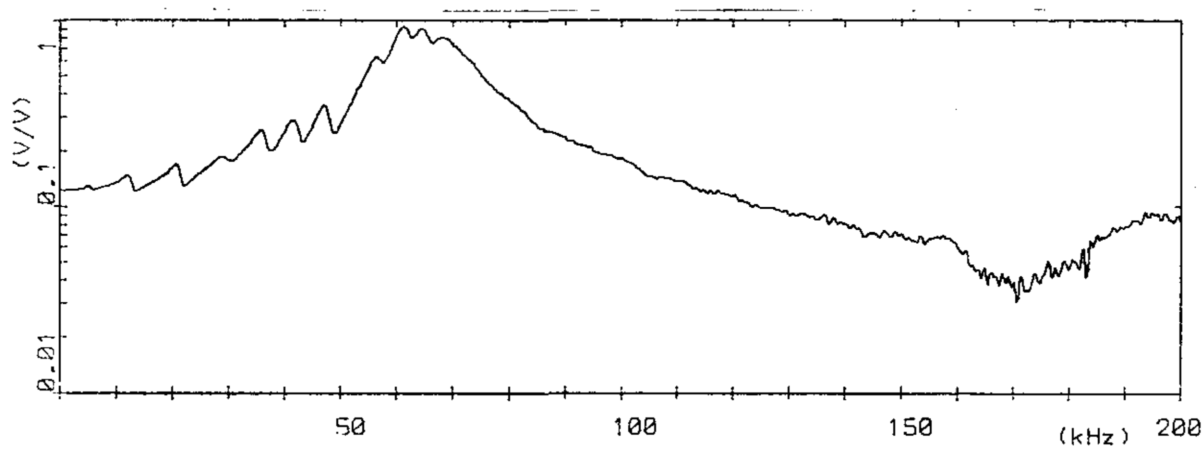

***Figure 24**: Transfer h.v.S to l.v.S; absolute value*

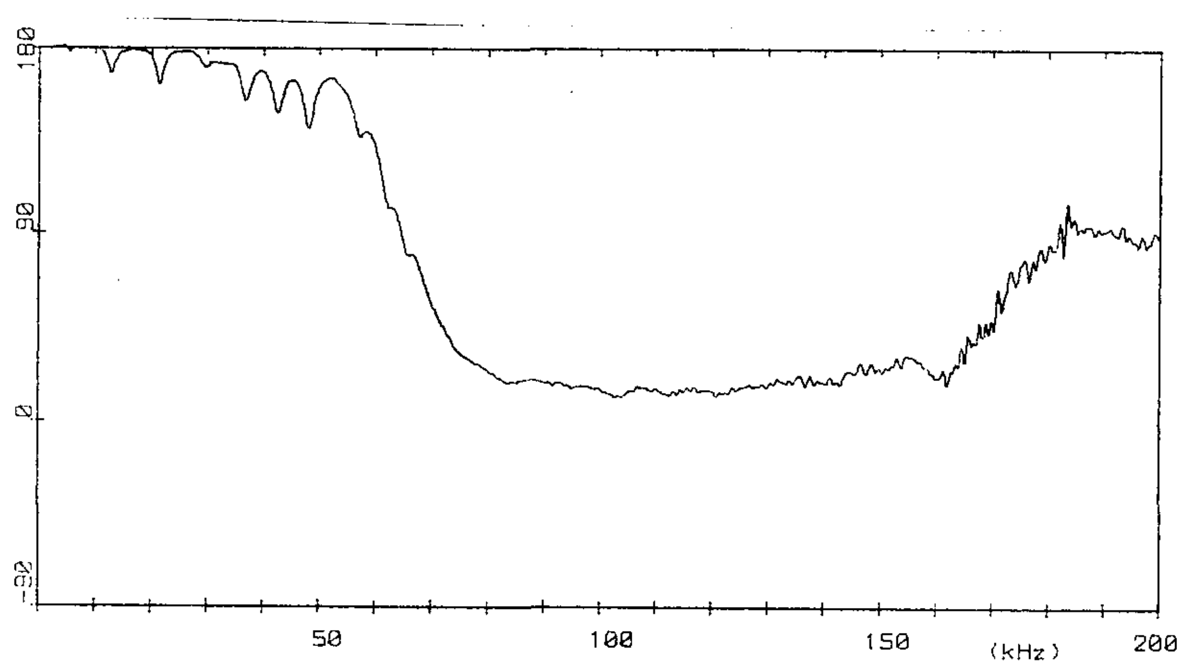

***Figure 25**: Transfer h.v.S to l.v.S; argument*

The transfer h.v.S to l.v.S is given in figure 24 (absolute value) and figure 25 (argument).

At low frequencies the voltage-ratio is equal to 1:8 with a phaseshift of 180°. The voltage transfer slowly increases, up to a maximum at about 60 kHz, the argument turns from 180° to 0°.

At 170 kHz the absolute value shows a flat minimum, whereby the argument turns to 90°. The model presented in 4.1 gives an explanation for the maximum at 60 kHz, but not for the minimum at 170 kHz.

Superimposed on this "large-scale" behaviour are minima and maxima up to 65 kHz. The argument shows small dips at these resonances.

A maximum in the imaginary part of the transfer always coincides with a maximum in the real part of the admittance on the h.v. side, in no-load as well as in short-circuit situation.

3.4. Transfer from h.v. center leg to h.v. outside leg.

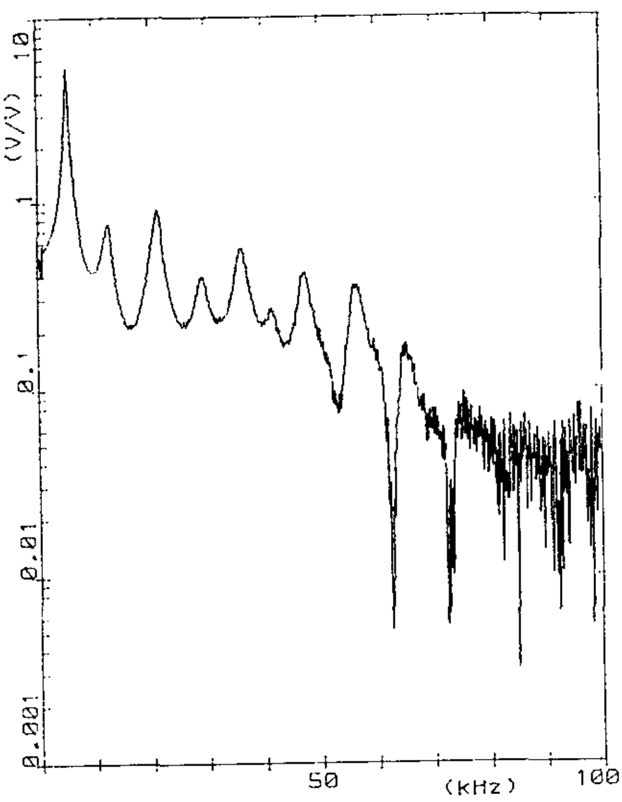

Figure 26: ***h.v.S to h.v.R; absolute value***

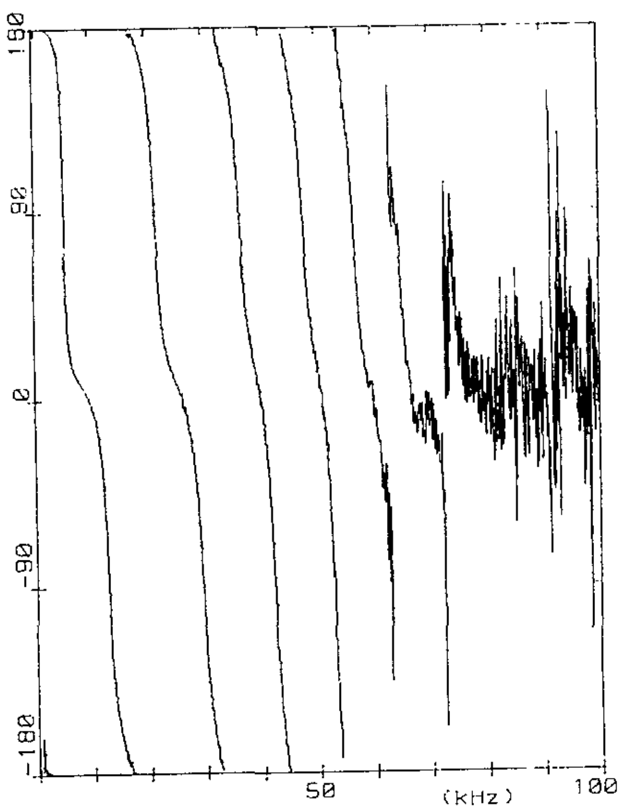

Figure 27: ***Argument.***

Figure 26 and 27 give absolute value and argument respectively of the transfer h.v.S to h.v.R. The overall absolute value decreases up to about 70 kHz, to become constant for higher frequencies. The argument starts at 180° because the flux direction in the measured winding is opposite to the flux direction in the excited winding. After some fast changes in argument it stabilises at 0° above 70 kHz. Here the transfer becomes solely capacitive.

Again minima and maxima are visible below 70 kHz. A maximum of the transfer h.v.S to h.v.R coincides with a maximum of the input h.v.S. Because the transfer below some tens of kHz is mainly through the iron flux one can conclude that a maximum input current means a maximum iron flux.

Figure 28 gives the polar diagram for the transfer h.v.S to h.v.R. Each peak in figure 26 corresponds to a loop in figure 28. The peak around 5 kHz is too high to fit in this figure, only a small part of the corresponding loop is visible.

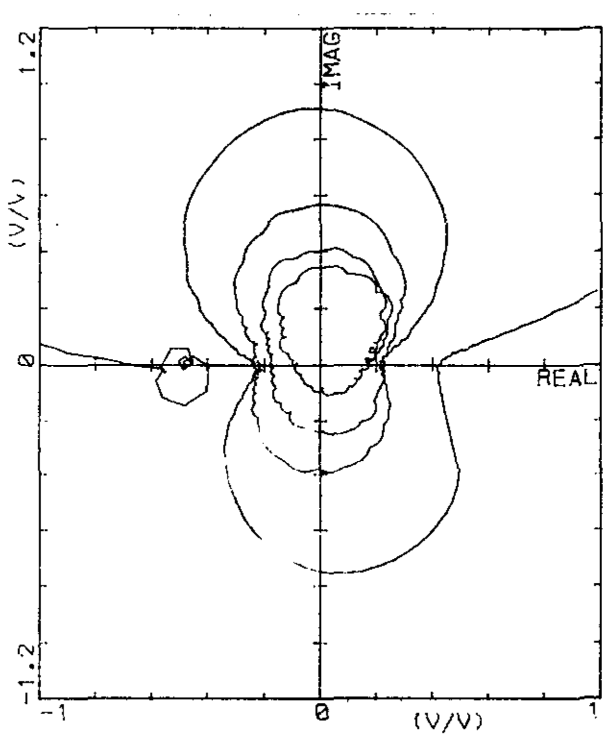

Figure 28: *h.v.S to h.v.R; polar diagram*

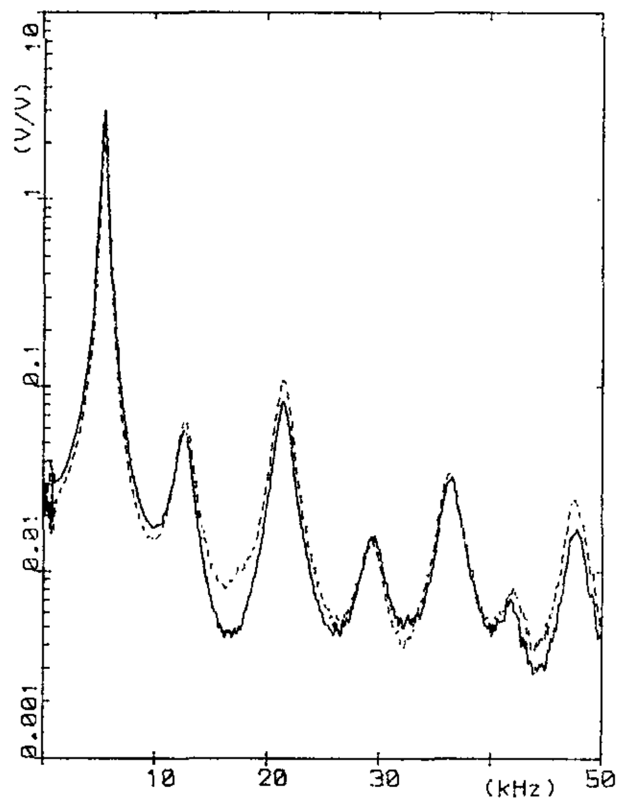

Figure 29: *Comparison between h.v.S to h.v.R and h.v.S to h.v.T*

The absolute values of the transfer h.v.S to h.v.R (solid line) and h.v.S to h.v.T (dotted line) are given in *figure 29*. Both are almost equal. Also for other transfers and admittances the differences between the outside legs are small. So further only the results for one outside leg will be presented.

The absolute values of the transfers to both outside legs also have been measured for some stationary frequencies as shown in *figure 30*. At low frequencies the transfer to each winding is approximately 50%. The flux produced in the center leg divides into two almost equal parts. Some small differences can be seen between both legs.

The minimum in both transfers is caused by resonance of the h.v. windings on the outside legs. A current is flowing in these h.v. windings due to the series resonance between inductance and capacitance. This current causes a reverse flux diminishing the voltage across the winding. This reverse flux closes largely through air.

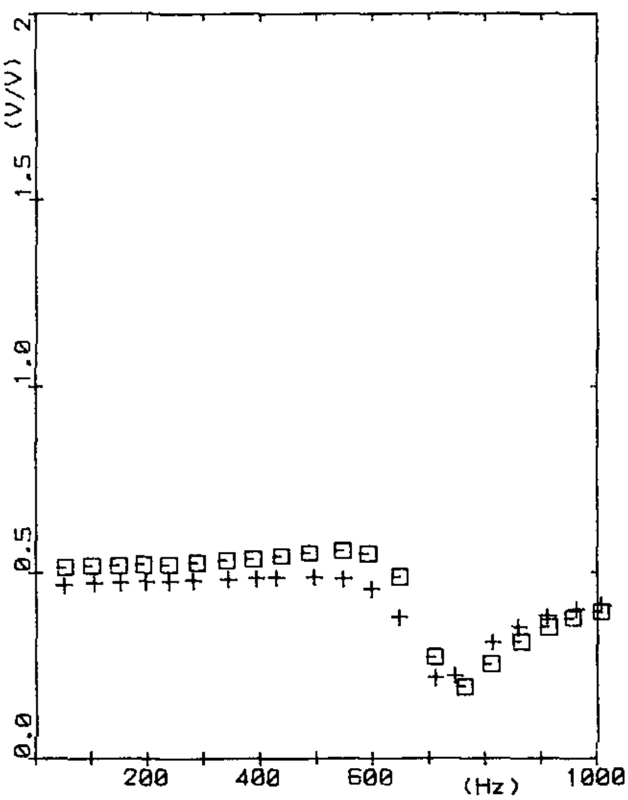

***Figure 30:** Absolute value of h.v.S to h.v.R (crosses) and h.v.S to h.v.T (squares); measured at stationary frequencies.*

3.5. Transfer from h.v. center leg to l.v. outside leg.

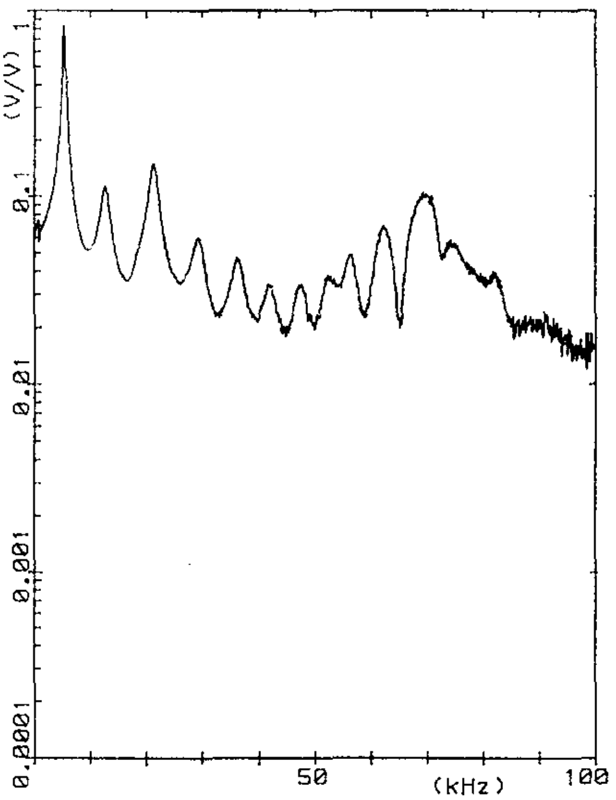

Figure 31: ***h.v.S to l.v.T; absolute value***

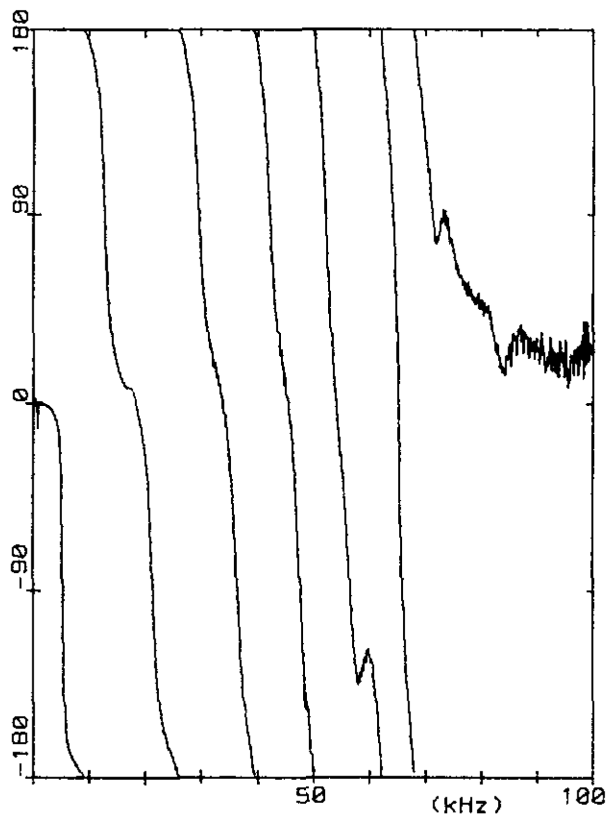

Figure 32: ***Argument***

The transfer h.v.S to l.v.T is given in figure 31 (absolute value) and figure 32 (argument). It resembles strongly the transfer h.v.S to h.v.R (figure 26 and 27). Both windings enclose the same iron flux. Small deviations are caused by the leakage flux that is gaining more influence at higher frequencies.

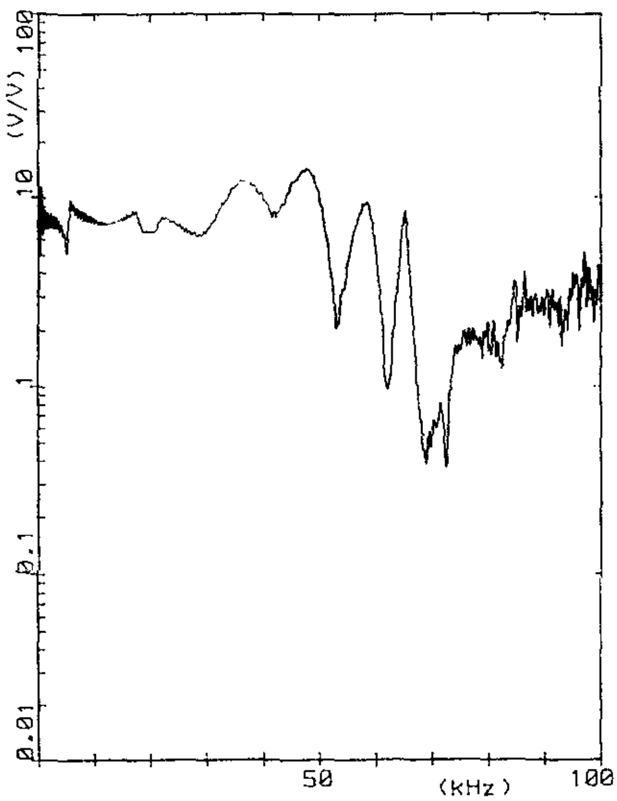

Figure 33: ***h.v.S to h.v.T divided by h.v.S to l.v.T; absolute value***

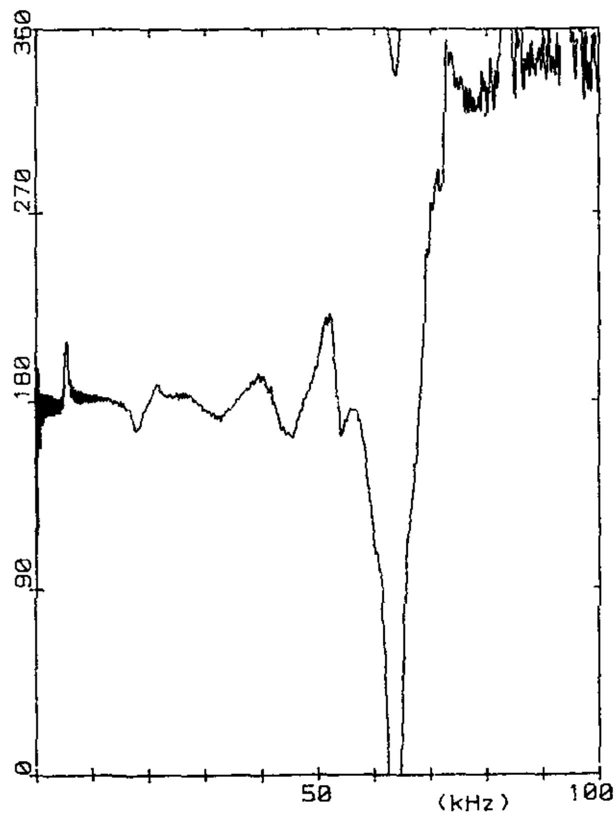

Figure 34: ***Argument***

To show the flux linkage the transfer h.v.S to h.v.T is divided by the transfer h.v.S to l.v.T. The results are given in figure 33 (absolute value) and figure 34 (argument).

The voltage ratio remains almost constant up to about 30 kHz. This constant is determined by the turns-ratio. Different resonances appear in both windings between 30 and 75 kHz. Because of this the voltage ratio shows strong oscillations in absolute value as well as in argument. Absolute value and argument become constant again above 75 kHz. The linkage between the windings has become solely capacitive in this frequency range.

From this one can conclude that the iron flux dominates over the leakage flux up to 30 kHz.

3.6. No-load admittance l.v. center leg.

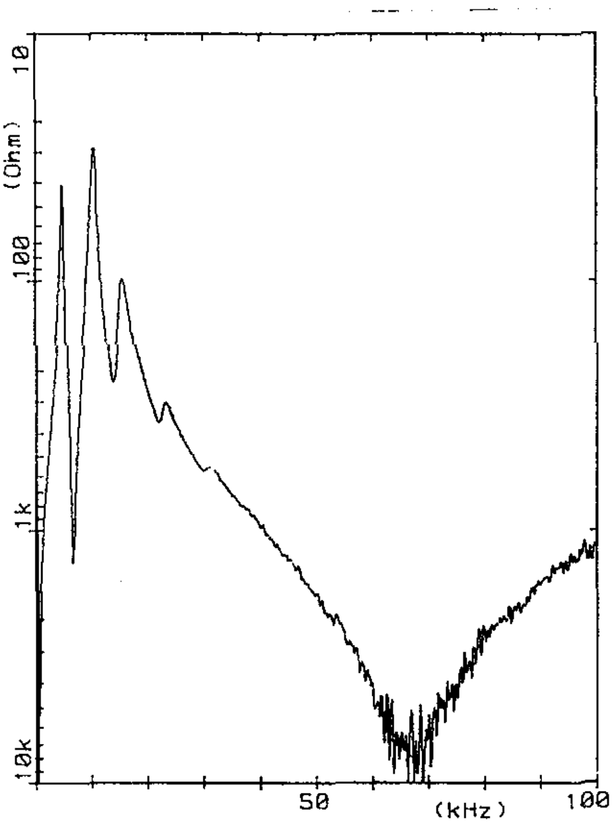

Figure 35: No-load l.v.S; abs. value

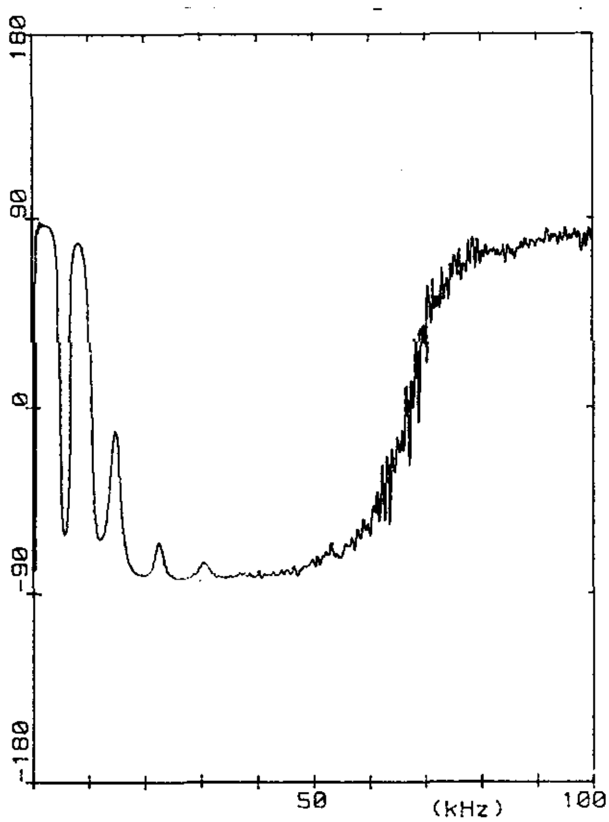

Figure 36: No-load l.v.S; Argument

The no-load l.v.S is shown in figure 35 (absolute value) and figure 36 (argument). At low frequencies the picture resembles the no-load h.v.S, as shown in figure 17 and 18: a fast decline of the absolute value up to 800 Hz; after that a repetition of minima and maxima. The resonant frequencies are slightly lower than those measured on the h.v. side. The overall view on l.v. side shows a minimum at 800 Hz, a maximum somewhere near 10 kHz and a minimum at 68 kHz. An explanation for this behaviour will be given in section 4.1.

3.7. Short-circuit admittance l.v. center leg.

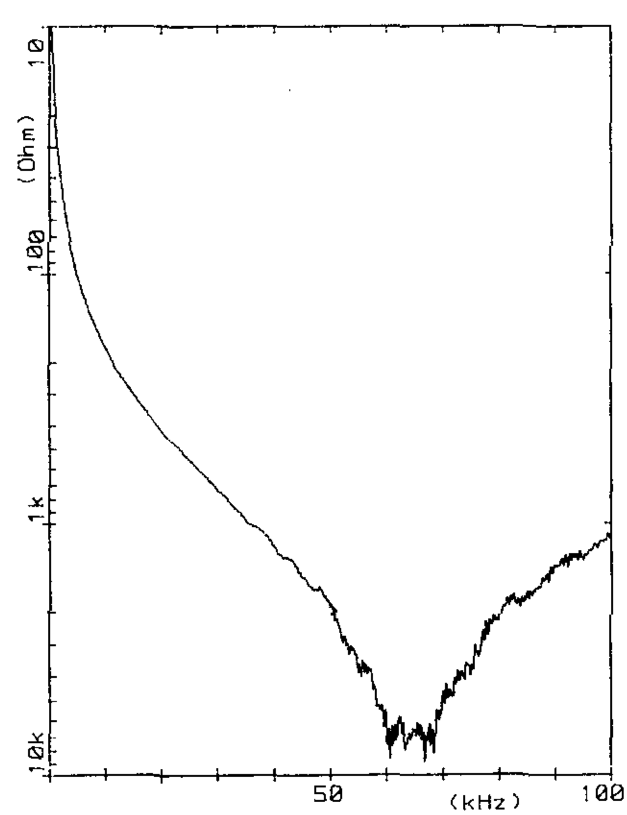

Figure 37: Short-circuit l.v.S; absolute value

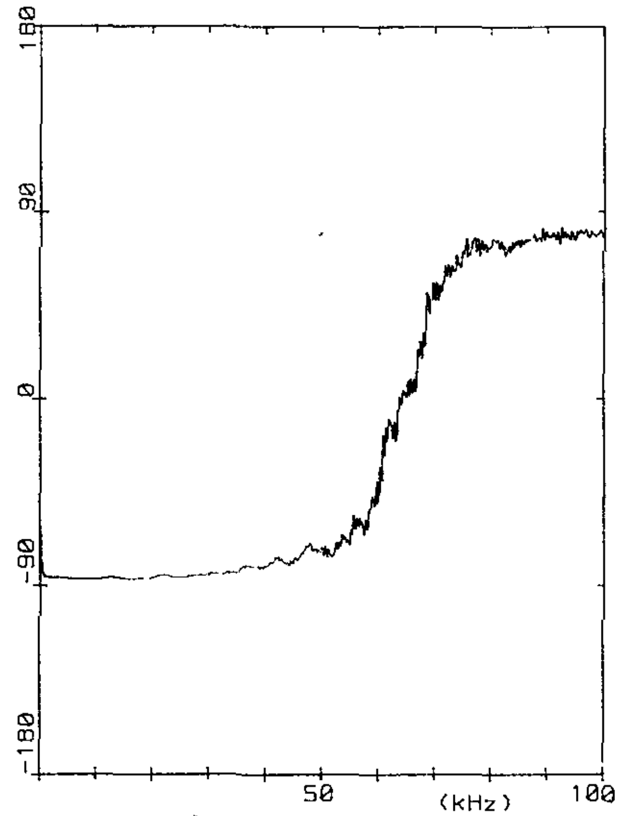

Figure 38: Short-circuit l.v.S; argument

Figure 37 and 38 give absolute value and argument respectively of the short-circuit l.v.S.

Unlike the other input admittances this one shows a simple behaviour. Up to 64 kHz one can see an inductive behaviour, the absolute value of the admittance diminishes and the argument is -90°. Above 64 kHz the behaviour is capacitive. No part-winding resonances are visible.

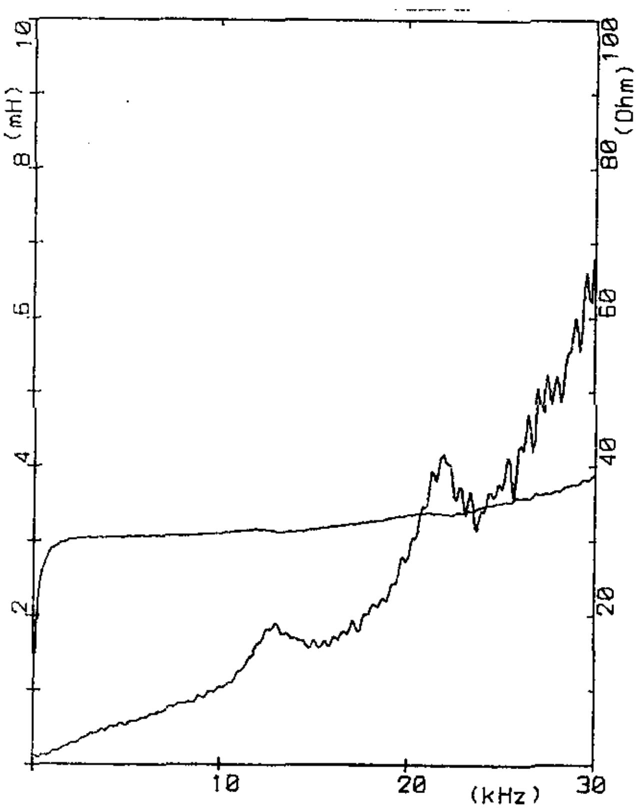

The absence of part-winding resonances makes it possible to determine resistance and inductance over a large frequency range.
Figure 39 gives resistance and inductance calculated from the measured admittance, assuming the latter can be represented as an R-L-series connection.
The inductance is constant and equal to 3.2 ± 0.1 mH. The resistance increases from 1 Ω at 200 Hz to 30 Ω at 20 kHz.
At 30 kHz the values become less accurate, due to the nearby resonance.

Figure 39: Resistance and inductance for R-L-series connection determined from short-circuit I.v.S

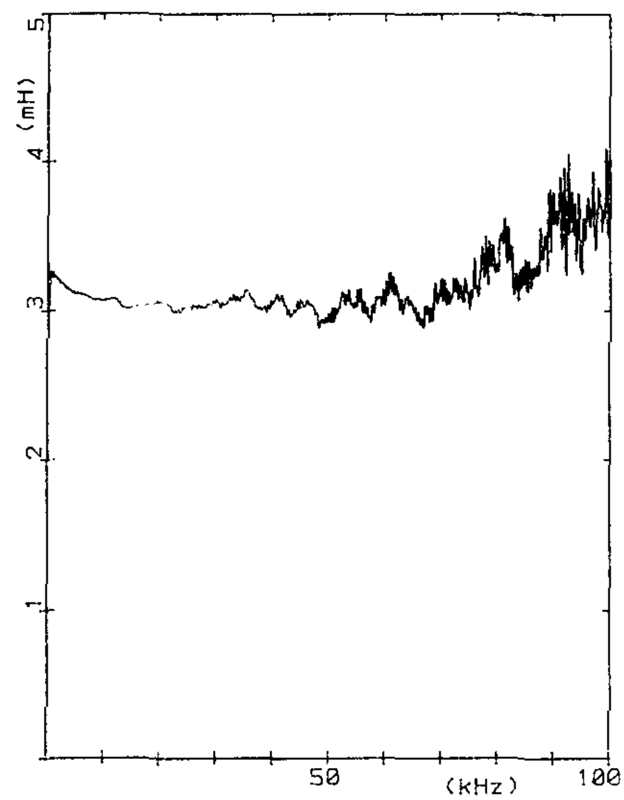

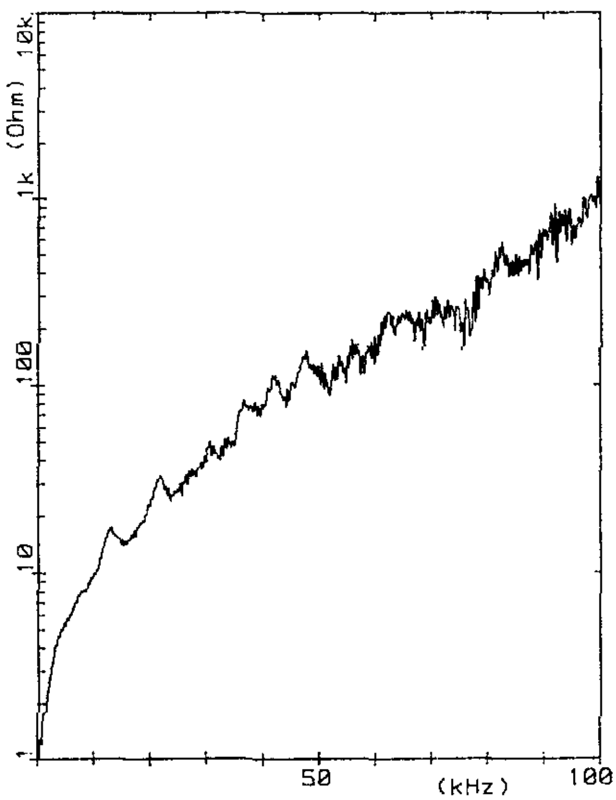

Figure 40: Inductance *Figure 41: Resistance*

for capacitance parallel to R-L-series connection

determined from short-circuit I.v.S

To correct for this effect a capacitor is assumed parallel to the series connection of inductor and resistor. The value of the capacitor has been found from the value of the inductor and the resonant frequency to be 1950 pF. The results are given in figure 40 (inductance) and figure 41 (resistance). The inductance is constant up to 100 kHz, and equal to 3.15 $\pm$ 0.05 mH. The resistance increases up to 1 kΩ at 100 kHz. This means that, for modelling purposes, the frequency dependence of the leakage inductance can be neglected, but the frequency dependence of the resistance representing the copper losses must be taken into account.

3.8. Transfer from l.v. to h.v. center leg.

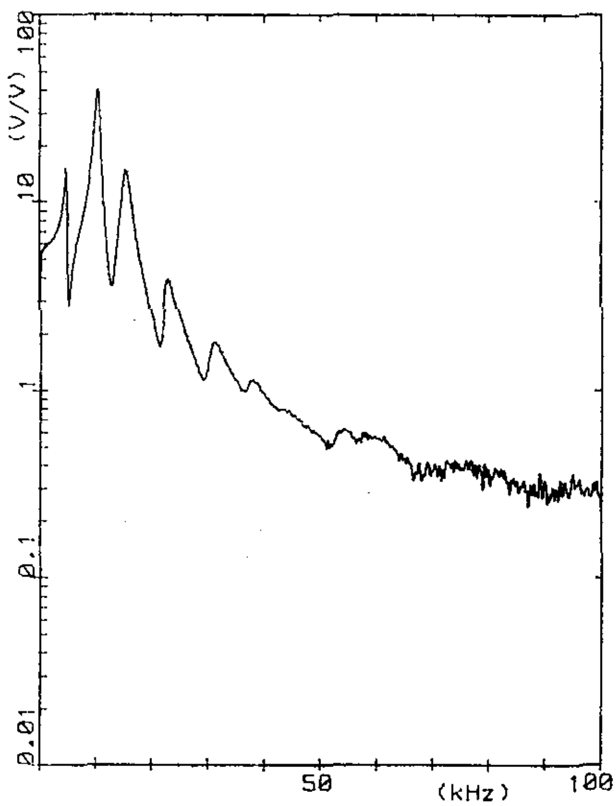

Figure 42*: *Transfer l.v.S to h.v.S absolute value

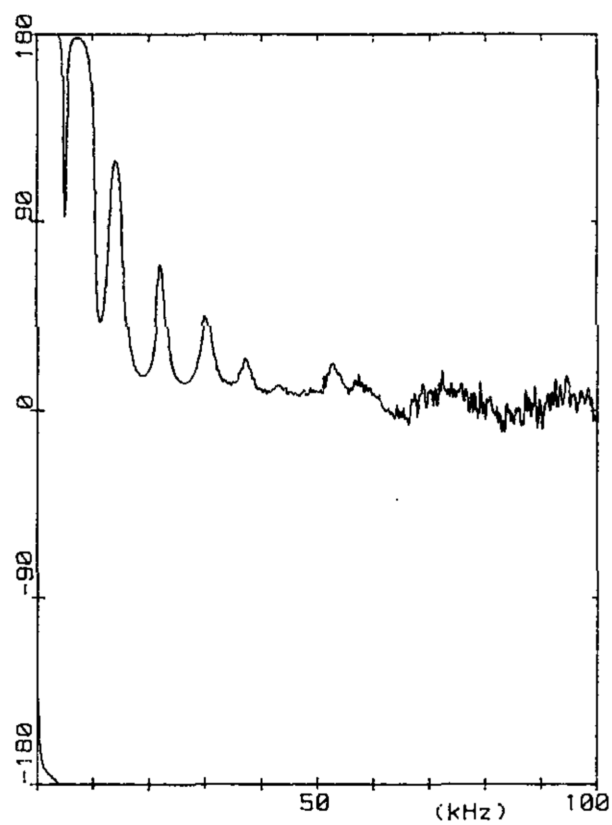

Figure 43*: *Transfer l.v.S to h.v.S argument

The transfer l.v.S to h.v.S is given in figure 42 (absolute value) and 43 (argument). The maxima of the transfer coincide with the maxima of the input admittance. The same phenomenon was observed on high-voltage side. Above 40 kHz the resonances disappear and the transfer stabilises at 0.3 V/V. The argument turns from 180° at low frequencies to 0° at high frequencies.

3.9. Transfer from l.v. center leg to l.v. outside leg.

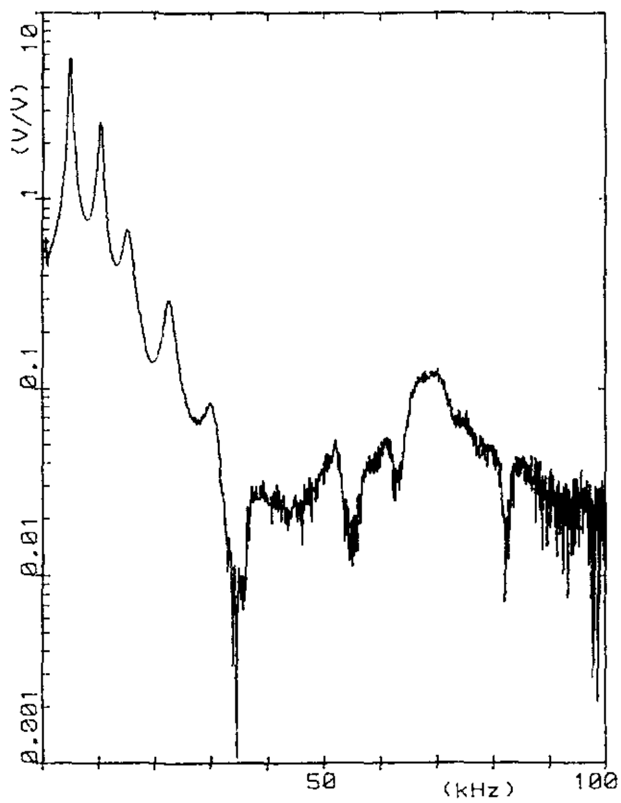

Figure 44: Transfer l.v.S to l.v.T absolute value

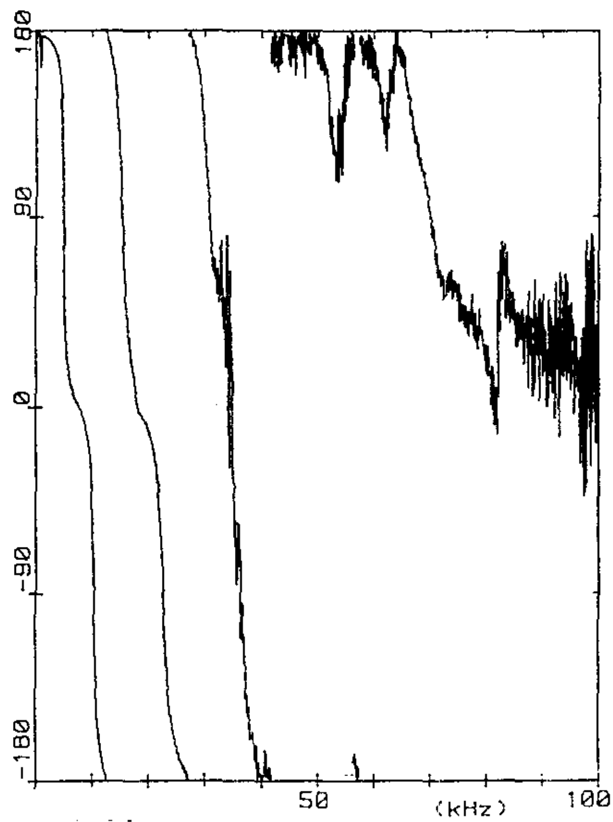

Figure 45: Transfer l.v.S to l.v.T argument

The transfer l.v.S to l.v.T is given in figure 44 (absolute value) and figure 45 (argument). It resembles the transfer h.v.S to h.v.R and h.v.S to l.v.R. The decline from the low-frequency (magnetic) transfer to the high-frequency (capacitive) transfer is steeper than with excitation of the h.v. winding (figure 31), because the magnetic transfer is N^2 times higher with excitation on l.v. side (N being the turns ratio). The capacitive transfer is of the same order of magnitude in both cases. The high-frequency transfer l.v.S to l.v.T is approximately 0.02 V/V.

3.10. Transfer from l.v. center leg to h.v. outside leg.

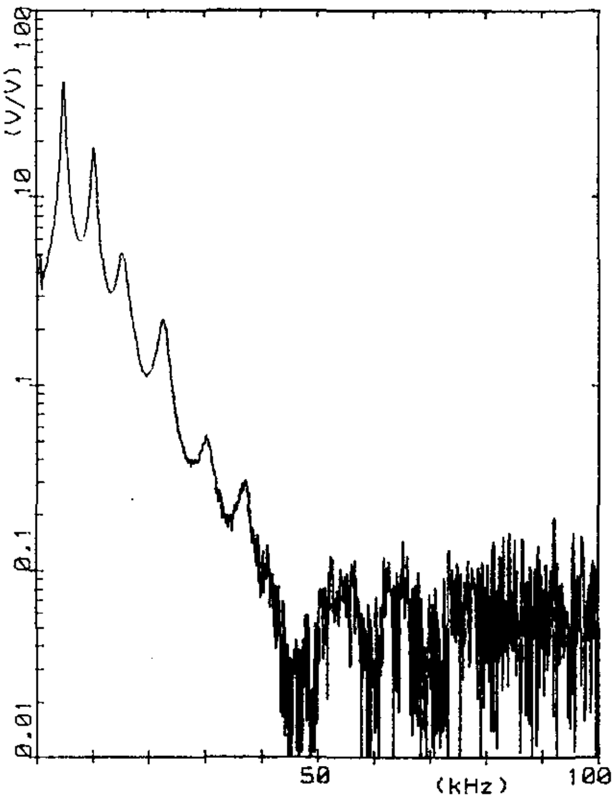

Figure 46: transfer l.v.S to h.v.T absolute value

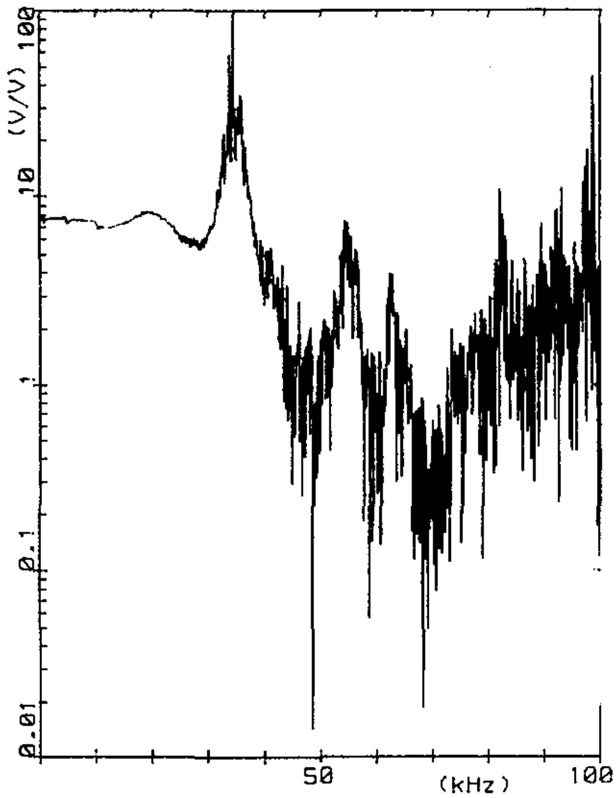

Figure 47: Flux linkage between h.v.T and l.v.T

The absolute value of the transfer l.v.S to h.v.T is given in figure 46. Up to about 30 kHz it is, apart from a constant factor, almost identical to the transfer h.v.S to l.v.T (3.9). The argument shows a steady decrease up to 40 kHz (not presented here). At higher frequencies the argument is not clearly defined because of the high noise-level.

The linkage between the h.v. side and the l.v. side can be observed in figure 47. The transfer l.v.S to h.v.T is divided by the transfer l.v.S to l.v.T. The absolute value of the result is given in figure 47. The quotient is constant up to 30 kHz. High-voltage and low-voltage windings resonate independently at higher frequencies because the iron flux no longer dominates the leakage flux.

3.11. No-load admittance h.v. outside leg.

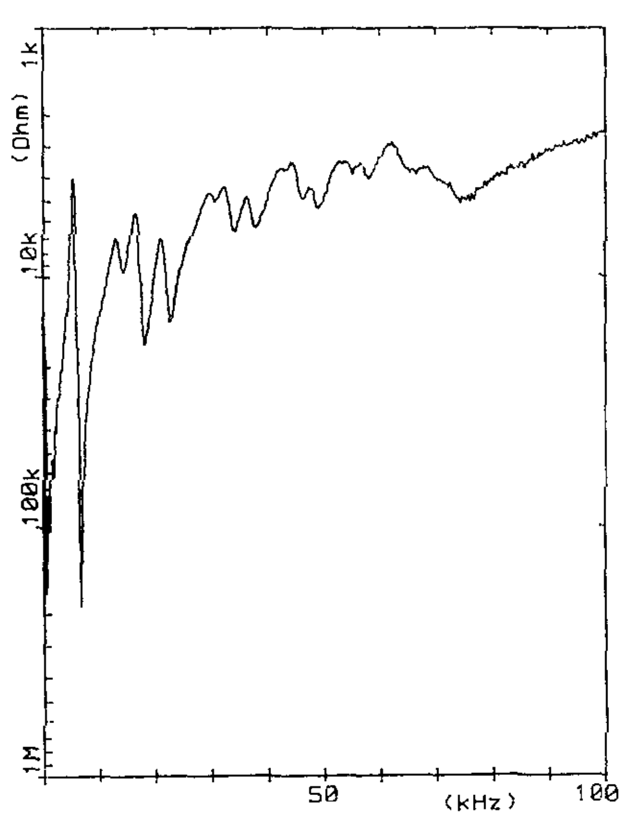

Figure 48: No-load h.v.T; absolute value

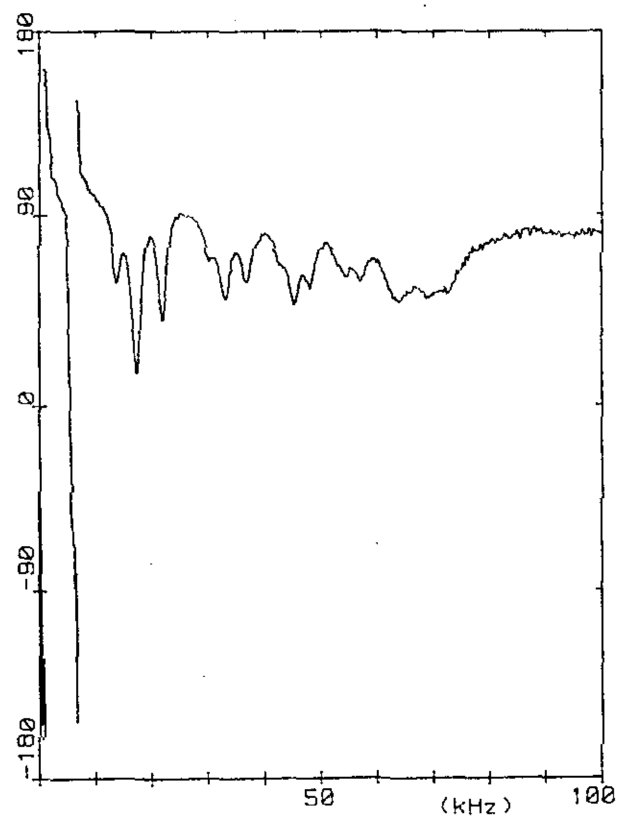

Figure 49: Argument

Figure 48 gives the absolute value of the no-load h.v.T; figure 49 gives the argument. The pattern is much more irregular than with excitation of the center leg. This means that the pattern of minima and maxima at least partly is caused by the non-excited legs. When exciting the center leg the non-excited legs are identical. This is not the case with excitation of an outside leg leading to the irregular pattern.

The overall behaviour of the three legs is nearly identical; a sharp admittance minimum below 1 kHz followed by a number of minima and maxima up to 70 kHz. The admittance of the outside legs resembles that of a capacitance of 900 pF above this frequency.

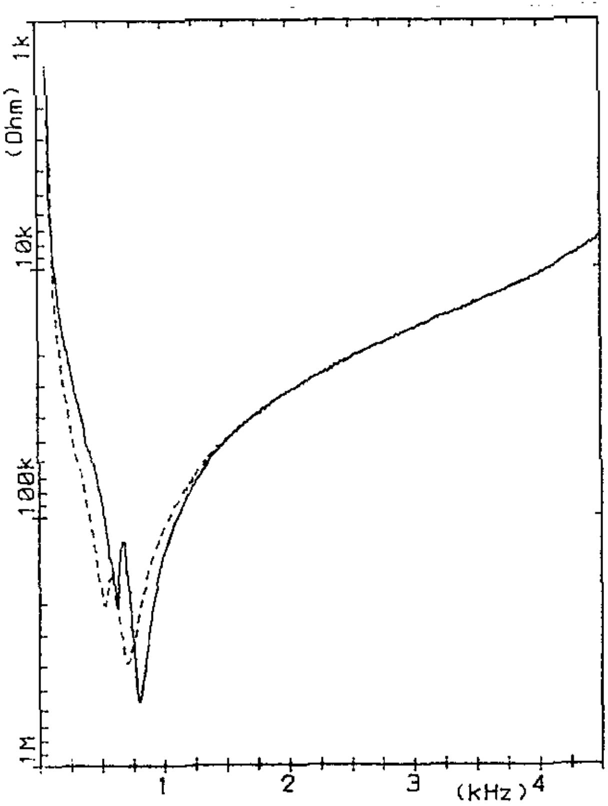

Figure 50: ***No-load h.v.T; absolute value measured with sweep generator***

Also for this leg the no-load admittance has been measured with a sweep generator with variable voltage amplitude. Figure 50 shows the absolute value of the no-load admittance up to 4500 Hz. The two curves are for effective values of the input voltage of 2 Volt and 100 Volt (dotted line). A double peak between 500 and 800 Hz is clearly visible, just like the shift to lower frequencies for higher input voltages.
The double peak is caused by the different resonant frequencies of both unexcited high-voltage windings. In chapter 4 a model to explaine the double peak will be given.

The shift of the resonant frequency shows the increase in inductance at higher voltages. For frequencies above 1 kHz the impedance is independent of the applied voltage amplitude, for the amplitudes used. Application of higher voltage amplitudes will cause the resonant frequencies to shift to even lower values and may even cause differences for higher frequencies. But it seems to be save to say that above a few kHz there is no longer an influence of the vol tage amplitude on the admittance. Because the pulse measurements posses only a small amount of low frequencies, the magnitude and shape of the pulse have almost no influence on the derived frequency plots. This means that a low-voltage pulse can be used to predict the response on a high-voltage pulse and that the derived frequency plots are applicable for high-voltage modelling above a few kHz in no-load. In short-circuit situation the plots are applicable for all frequencies.

3.12. Short-circuit admittance h.v. outside leg.

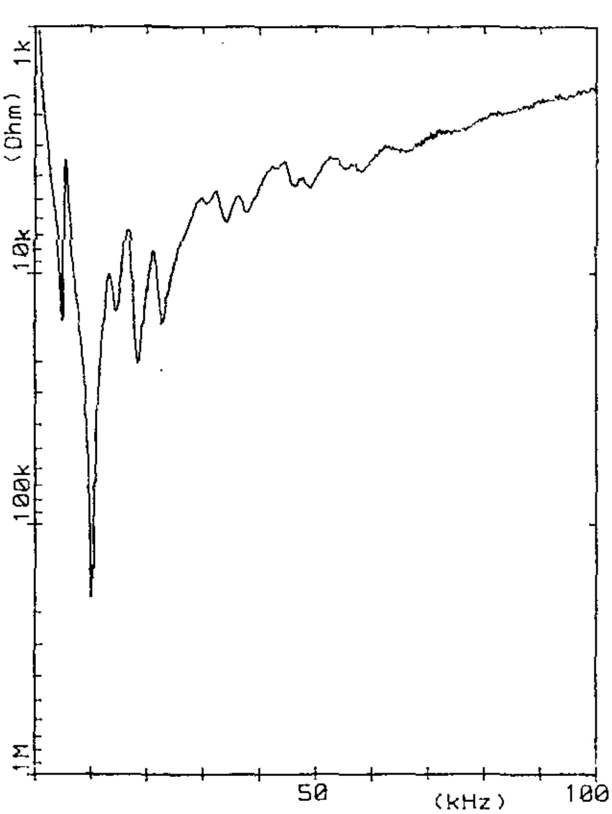

***Figure 51**: Short-circuit h.v.T absolute value*

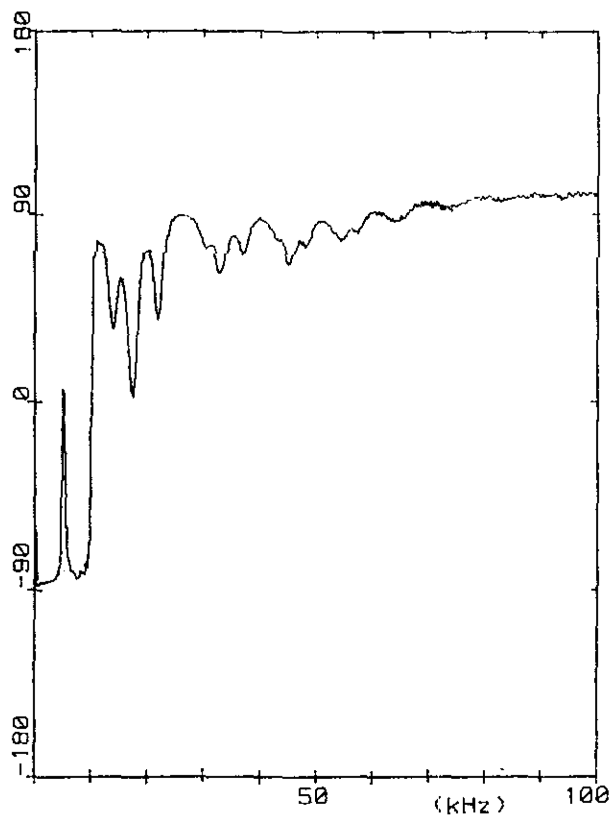

***Figure 52**: Short-circuit h.v.T argument*

The short-circuit h.v.T is given in figure 51 (absolute value) and figure 52 (argument). Again the same differences between the center leg and the outside leg as in the no-load admittance are visible. The overall pattern is the same but the pattern of part-winding resonances is more irregular. In short-circuit situation the differences are smaller. Up to 12 kHz and above 62 kHz the behaviour of the windings is identical.

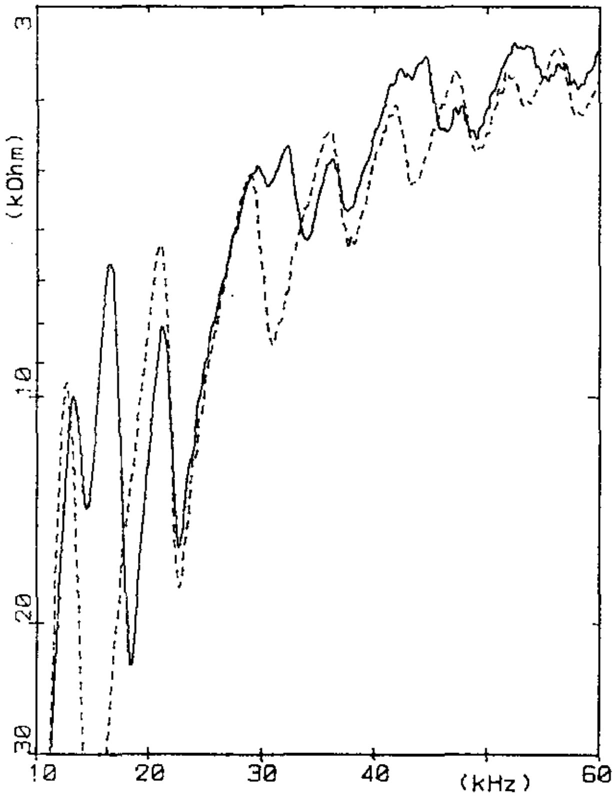

Between 12 kHz and 62 kHz the resonant frequencies of the center leg also appear in the outside leg. Extra maxima appear in the outside leg between the second and the third maximum, between the fourth and the fifth, between the sixth and the seventh and between the eighth and the ninth.

Figure 53 gives the absolute values of the short-circuit admittance for both windings in the frequency range of 10 kHz to 60 kHz. The solid line is for an outside leg, the dotted line for the center leg.

Figure 53: Short-circuit h.v.T (solid line) and short-circuit h.v.S (dotted line)

3.13. Transfer from h.v. to l.v. outside leg.

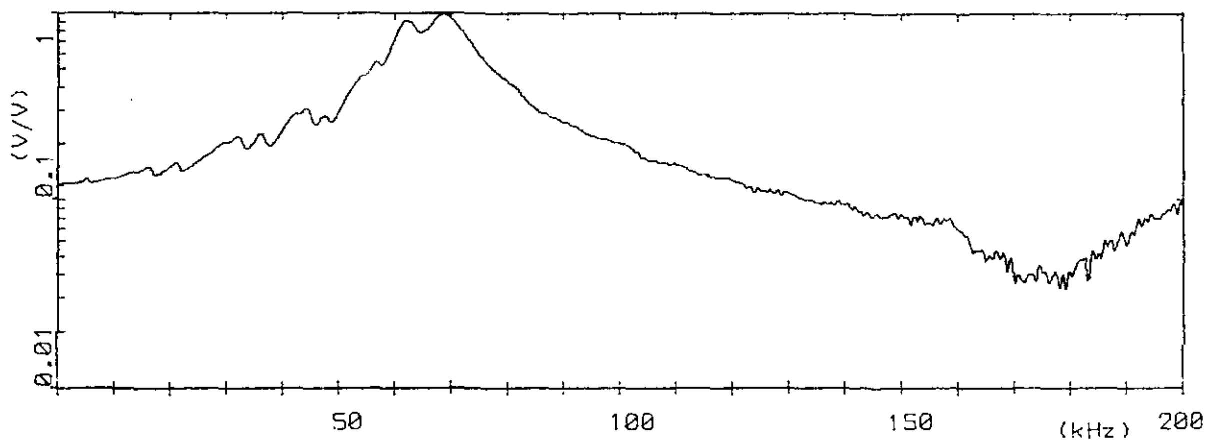

Figure 54 Transfer h.v.T to l.v.T; absolute value

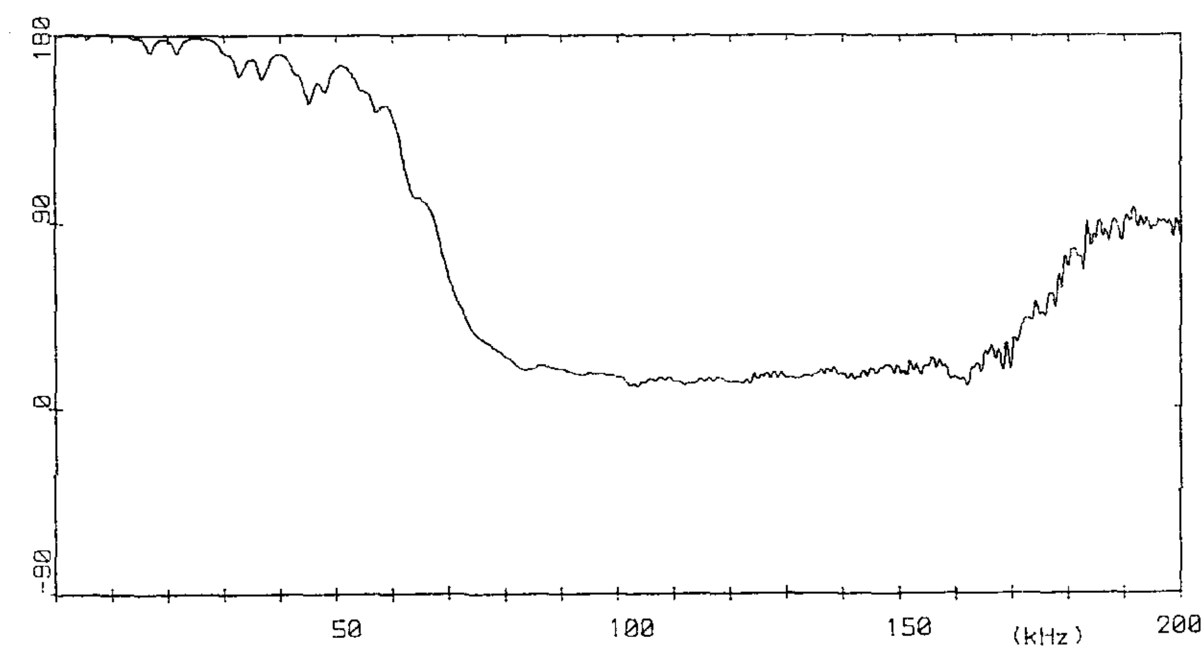

Figure 55: Transfer h.v.T to l.v.T; argument

The transfer h.v.T to l.v.T is shown in figure 54 (absolute value) and figure 55 (argument) The absolute value possesses a maximum at 64 kHz and a minimum at 170 kHz. Again minima and maxima are superimposed on this overall behaviour. A maximum in transfer always coincides with a maximum in input admittance.

3.14. Transfer from h.v. outside leg to center leg.

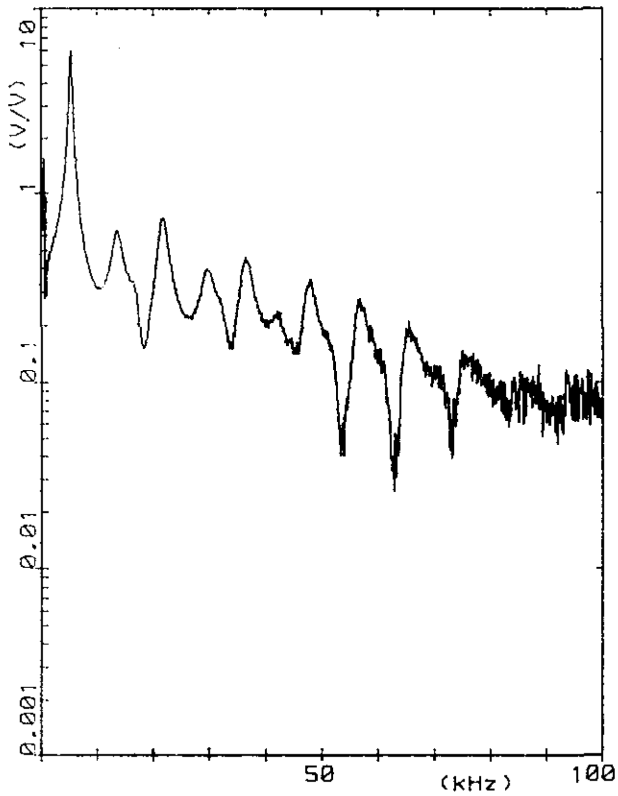

Figure 56: Transfer h.v.R to h.v.S absolute value

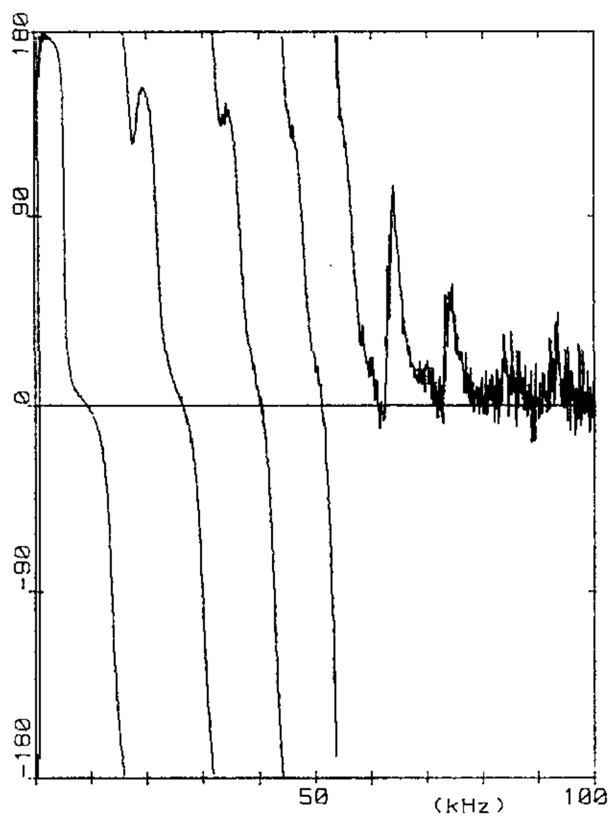

Figure 57: Transfer h.v.R to h.v.S argument

The transfer h.v.S to h.v.R is given in figure 56 (absolute value) and figure 57 (argument). The absolute value shows a number of maxima and minima. A maximum in transfer coincides with a maximum in the admittance up to 48 kHz. The admittance maxima at 53 kHz and 62 kHz coincide with minima in transfer. The minimum at 74 kHz has no corresponding feature in the admittance. Above 85 kHz the transfer is solely capacitive and equal to about 0.08V/V.

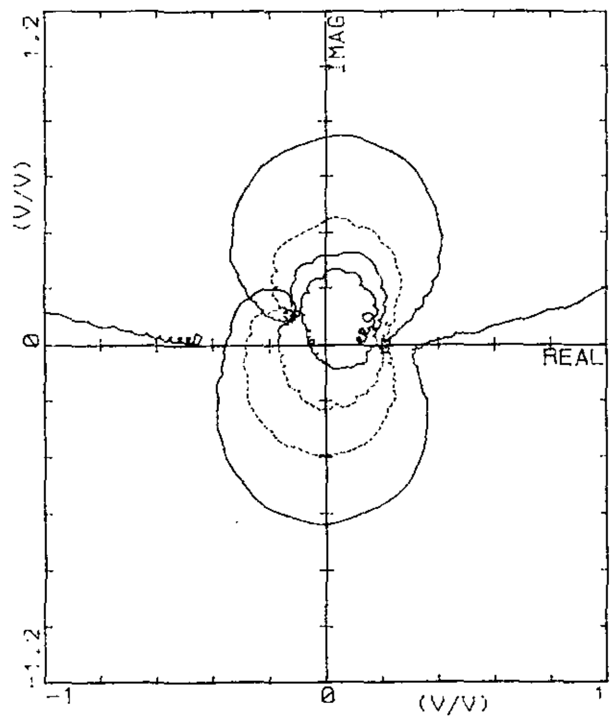

Figure 58: *transfer h.v.R to h.v.S; polar diagram*

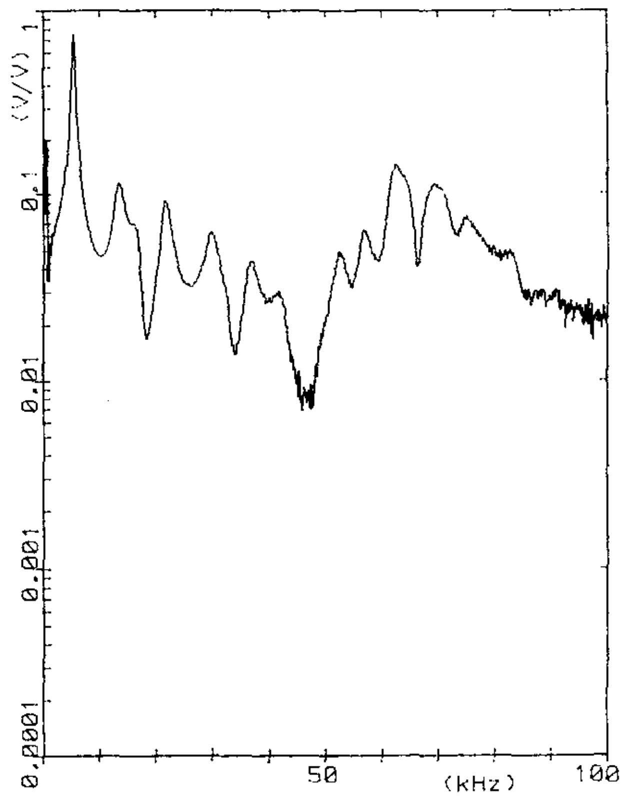

Figure 59: *transfer h.v.R to l.v.S absolute value*

Figure 58 gives the polar diagram for the transfer h.v.R to h.v.S in the frequency range of 1 kHz up to 50 kHz.

The absolute value of the transfer h.v.R to l.v.S is given in figure 59. It is equivalent to the transfer h.v.R to h.v.S (figure 56) up to 43 kHz. The linkage between h.v and l.v. disappears at higher frequencies. Where the transfer h.v.R to h.v.S shows an overall decreasing behaviour with increasing frequency, the transfer h.v.R to l.v.S shows a broad maximum around 65 kHz. The transfer h.v.S to l.v.S also is maximal at this frequency. The transfer h.v.R to l.v.S slowly decreases above 80 kHz, and reaches the final value of approximately 1:100 at 150 kHz.

3.15. Transfer from h.v. outside leg to other outside leg.

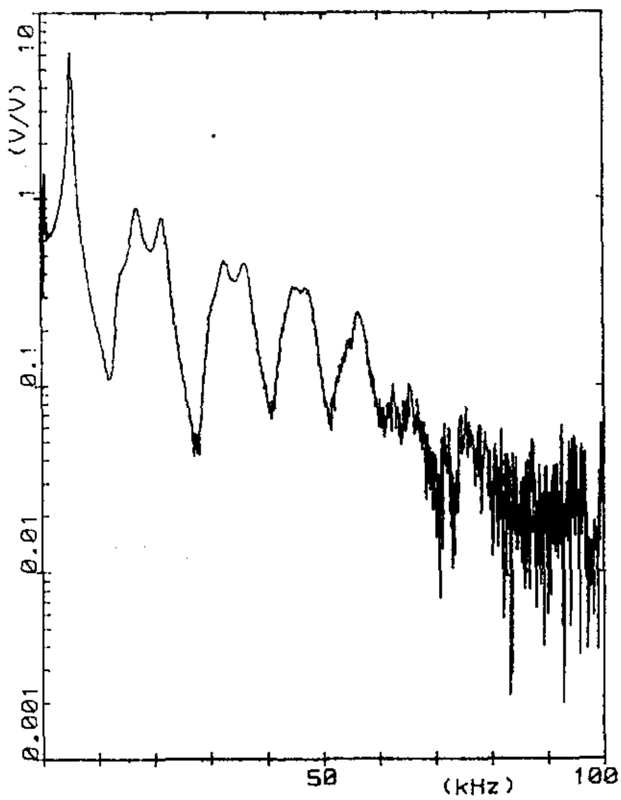

Figure 60: Transfer h.v.R to h.v.T absolute value

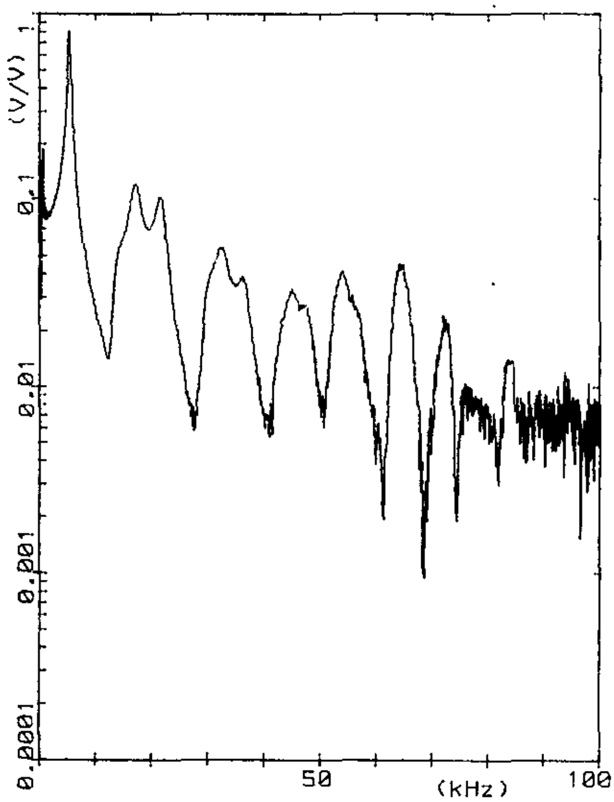

Figure 61: Transfer h.v.R to l.v.T absolute value

Figure 60 gives the absolute value of the transfer h.v.R to h.v.T. Figure 61 gives the transfer h.v.R to l.v.T. Both behave the same up to 55 kHz. H.v. and l.v. winding are no longer connected by the iron flux above that frequency. It is remarkable that the linkage in this case remains up to 55 kHz, but in case of transfer to the center leg (3.14) the linkage between h.v. and l.v. side remains only up to 43 kHz. The value of the transfer for high frequency (above 100 kHz) is approximately 0.01 V/V for h.v.R to h.v.T and 0.003 V/V for h.v.R to l.v.T.

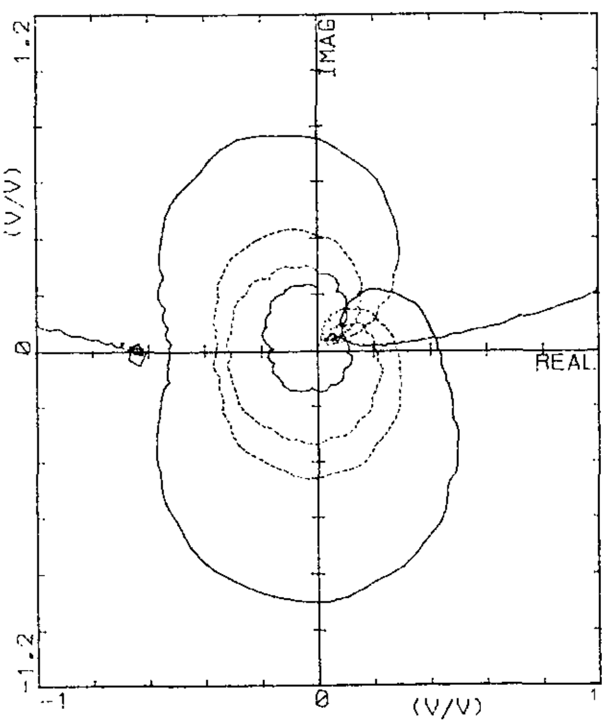

Figure 62: Transfer h.v.R to h.v.T polar diagram

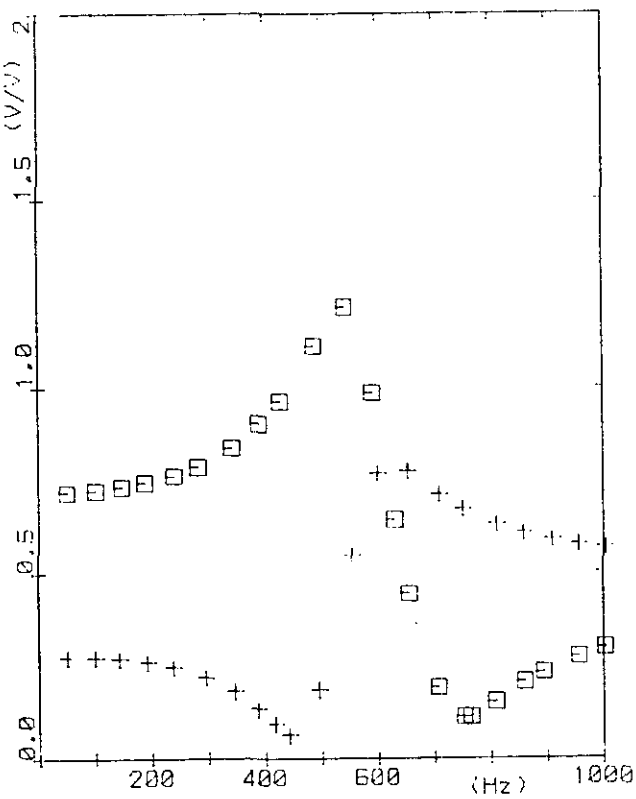

Figure 63: h.v.R to h.v.T (crosses) and h.v.R to h.v.S (squares)

Figure 62 gives the polar diagram for the transfer h.v.R to h.v.T in the frequency range of 1 kHz up to 50 kHz. Figure 63 gives the transfer h.v.R to h.v.T (crosses) and the transfer h.v.R to h.v.S (squares), as measured at stationary frequency. The transfer to h.v.S shows a maximum at 550 Hz and a minimum at 750 Hz. The transfer to h.v.T shows a minimum at 200 Hz and a maximum at 600 Hz. In chapter 4 an explanation for this behaviour will be given.

3.16. Input admittance l.v. outside leg.

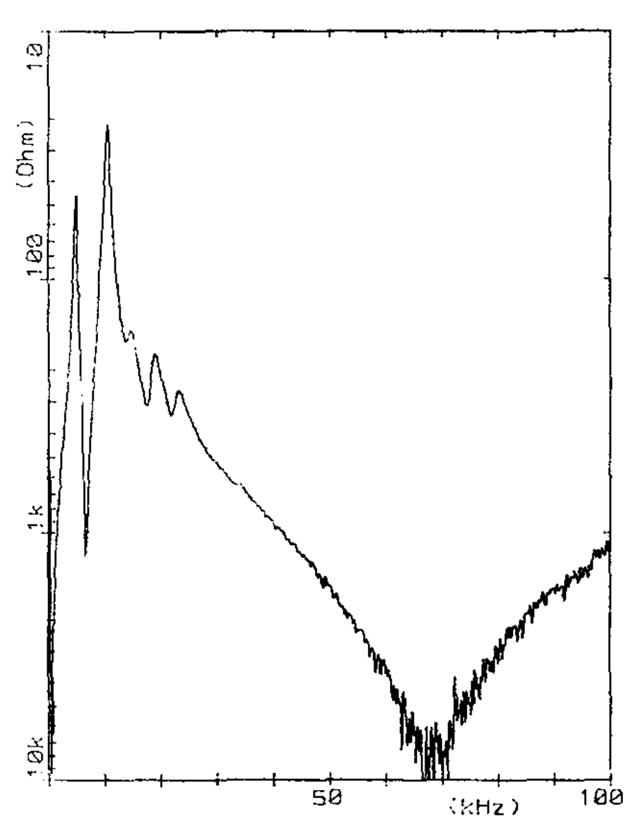

Figure 64: No-load l.v.T; absolute value

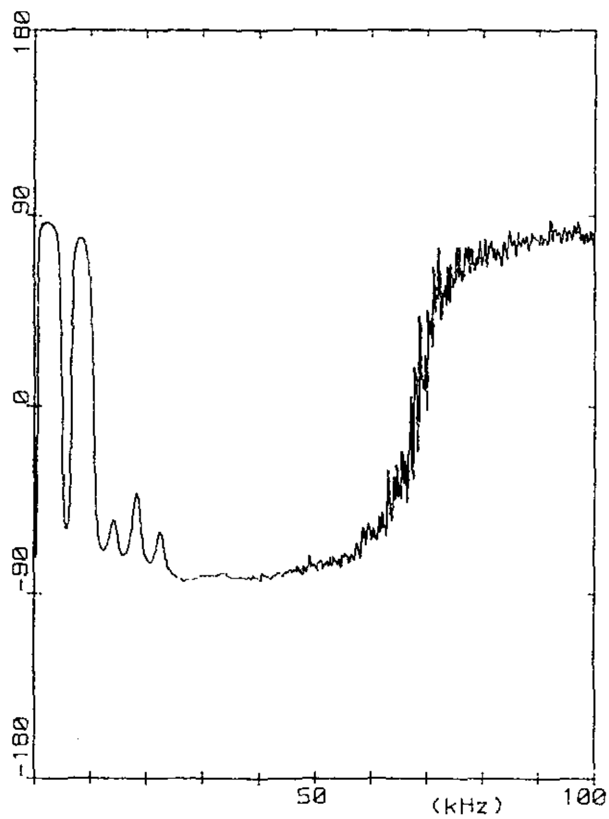

Figure 65: No-load l.v.T; argument

The no-load l.v.T is given in figure 64 (absolute value) and figure 65 (argument). The behaviour resembles that of the no-load l.v.S. Differences arise in the frequency range 12 to 32 kHz because of the different resonant frequencies. The short-circuit l.v.T (not presented here) is identical to the short-circuit l.v.S.

3.17. Transfer from l.v. to h.v. outside leg.

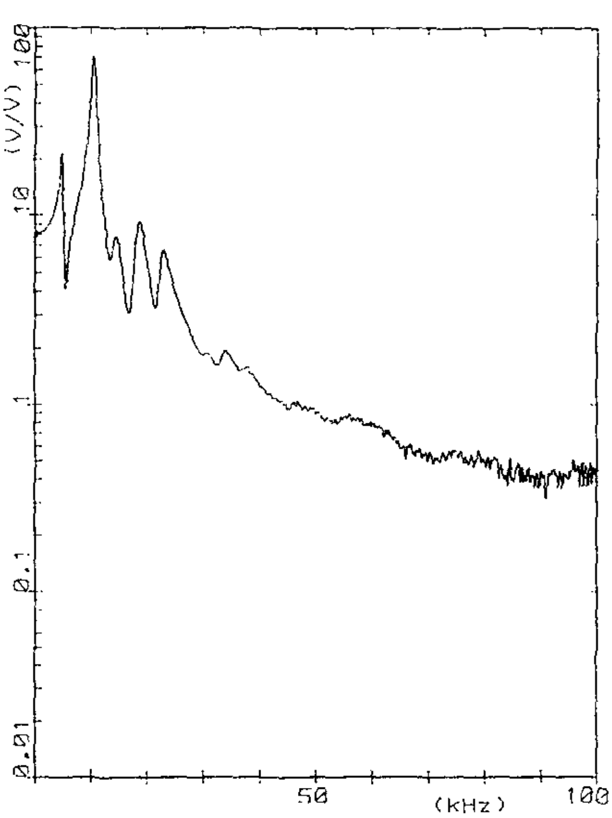

Figure 66: Transfer l.v.T to h.v.T absolute value

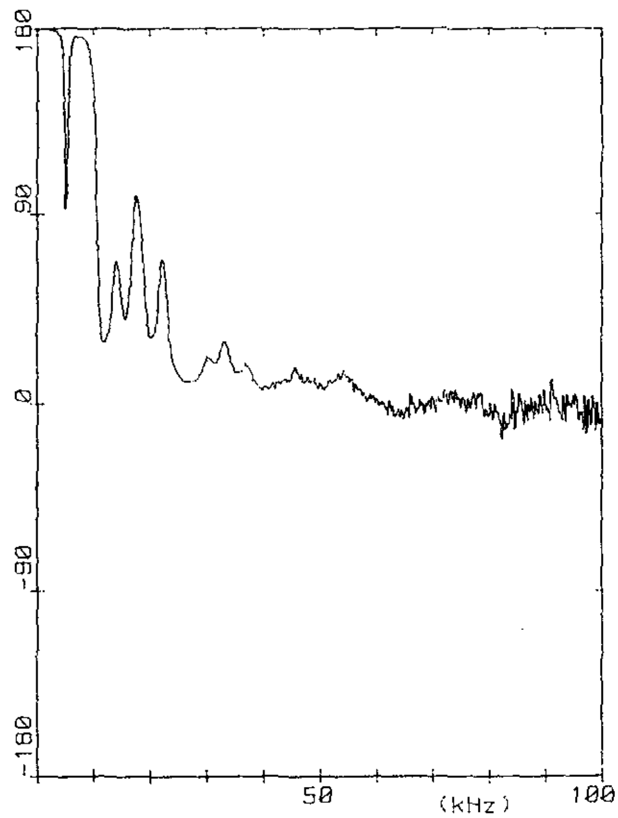

Figure 67: Transfer l.v.T to h.v.T argument

The transfer l.v.T to h.v.T is given in figure 66 (absolute value) and figure 67 (argument). The transfer is approximately equal to 8:1 at low frequencies. It is equal to a value of 1:25 at 100 kHz. Again the differences between this leg and the center leg are the different resonances between 12 kHz and 36 kHz.

3.18. Transfer from l.v. outside leg to other legs.

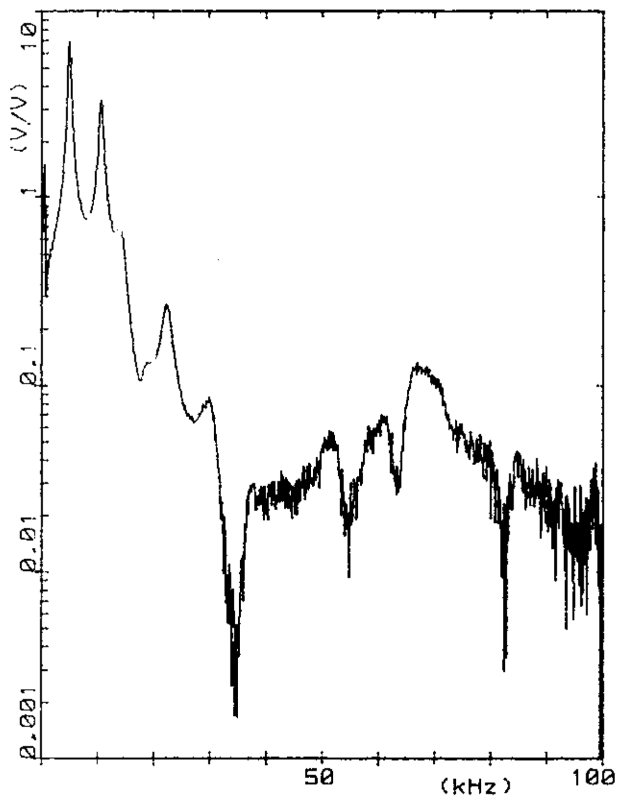

Figure 68 Transfer l.v.R to l.v.S
absolute value

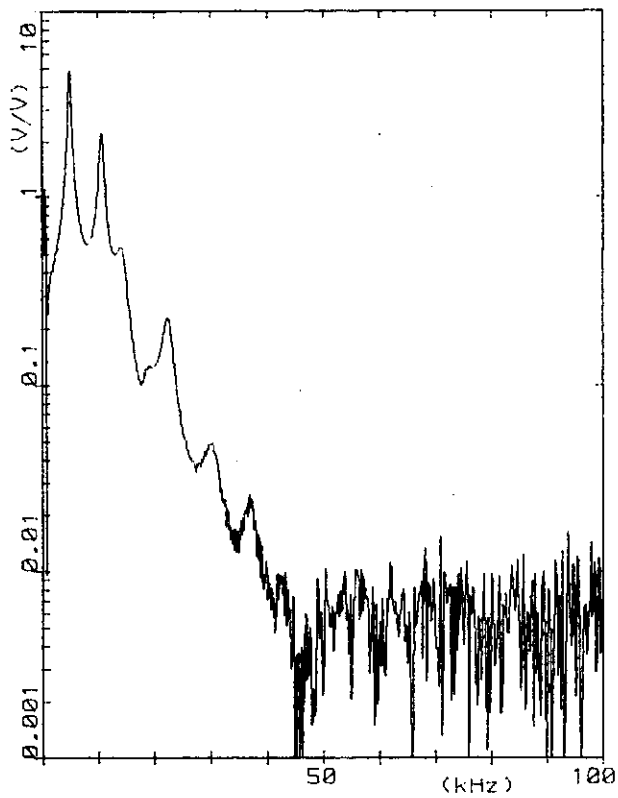

Figure 69: Transfer l.v.R to h.v.S
absolute value

The transfer from the low-voltage side resembles the transfer from the high-voltage side. The main difference is the ratio between low-frequency transfer and high-frequency transfer, because the turns-ratio is important at low frequencies, but not at high frequencies.

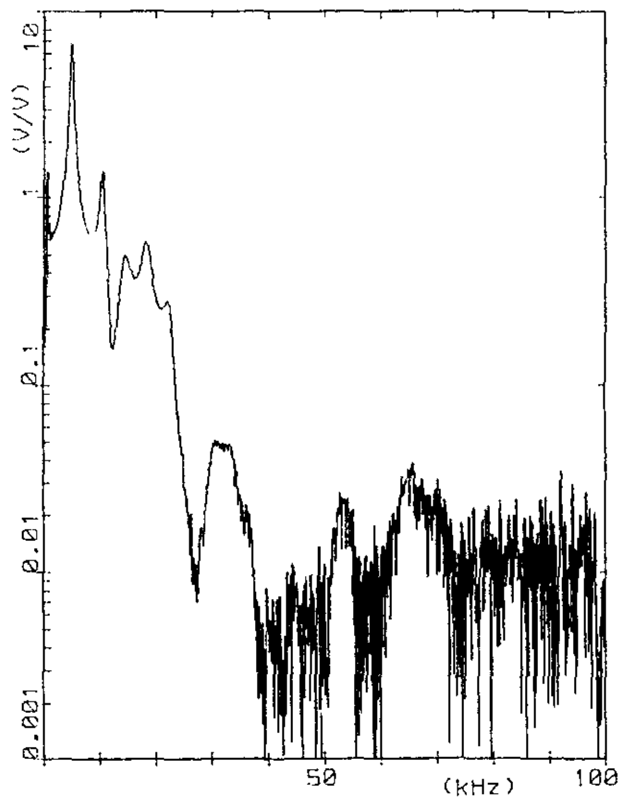

Figure 70: ***Transfer l.v.R to l.v.T absolute value***

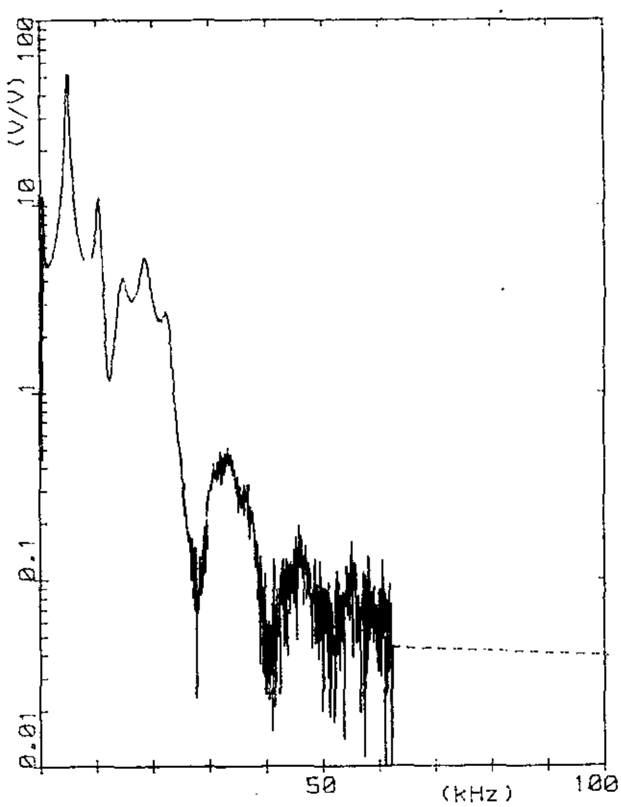

Figure 71: ***Transfer l.v.T to h.v.R absolute value***

Figure 68 gives the absolute value of the transfer l.v.R to l.v.S, figure 69 the absolute value of the transfer l.v.R to l.v.S, figure 70 the absolute value of the transfer l.v.R to l.v.T and figure 71 the absolute value of the transfer l.v.T to h.v.R.

4. Some simple models to explain the observed behaviour.

4.1. Single-phase model.

A widely used model for each phase of a transformer for power frequency is shown in figure 72.

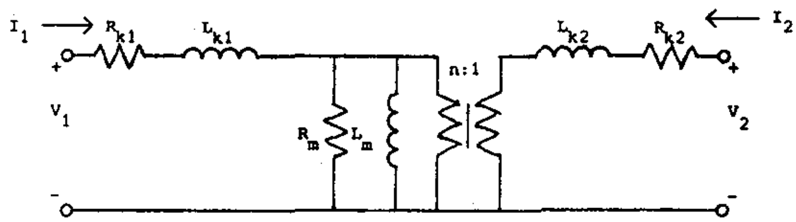

*Figure 72: **Low-frequency single-phase transformer model***

Here L_{k1} and L_{k2} are leakage inductances of the high-voltage and the low-voltage winding. L_m is the iron inductance rated to the high-voltage side. R_{k1} and R_{k2} represent the copper losses and R_m is determined by the iron loss. n is the turns-ratio.
Neglecting the losses gives the following equations:

$$v_1 = j\omega\,(L_{k1} + L_m) I_1 + j\omega\,\frac{L_m}{n}\,I_2 \tag{1}$$

$$v_2 = j\omega\,\frac{L_m}{n}\,I_1 + j\omega(L_{k2} + \frac{L_m}{n^2})\,I_2 \tag{2}$$

As a first approximation capacitances are added to represent the high-frequency behaviour, as shown in figure 73. The following equations hold for this case:

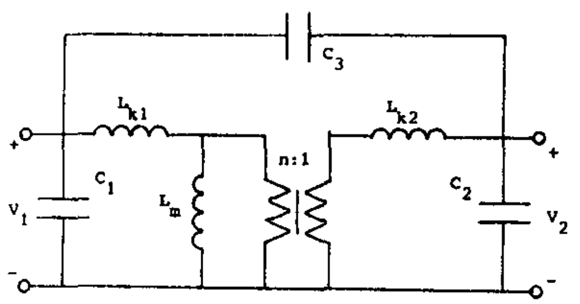

$$v_1 = Z_{11}\,I_1 + Z_{12}\,I_2 \tag{3}$$

$$v_2 = Z_{12}\,I_1 + Z_{22}\,I_2 \tag{4}$$

where

*Figure 73: **High-frequency model.***

$$Z_{11} = \frac{j\omega(L_{k1} + L_m) - j\omega^3(L_{k1} L_{k2} + L_m L_{k2} + L_m \frac{L_{k1}}{n^2})\ (C_2 + C_3)}{\Delta},$$

$$Z_{12} = \frac{j\omega \frac{L_m}{n} - j\omega^3(L_{k1} L_{k2} + L_m L_{k2} + L_m \frac{L_{k1}}{n^2})\ C_3}{\Delta}$$

$$Z_{22} = \frac{j\omega(L_{k2} + \frac{L_m}{n^2}) - j\omega^3(L_{k1} L_{k2} + L_m L_{k2} + L_m \frac{L_{k1}}{n^2})\ (C_1 + C_3)}{\Delta}$$

and.

$$\Delta = 1 - \omega^2\ [C_3\ \{L_m(1 - \frac{1}{n})^2 + L_{k1} + L_{k2}\} + C_1\ (L_m + L_{k1}) + C_2\ (\frac{L_m}{n^2} + L_{k2})]$$

$$+ \omega^4 (C_1C_2 + C_1C_3 + C_2C_3)\quad (L_{k1} L_{k2} + L_{k1} \frac{L_m}{n^2} + L_{k2} L_m)$$

From formula (3) and (4) equations can be derived for transfer fuctions and admittances.

No-load admittance on the high-voltage side (Figure 74)

$$\left.\frac{I_1}{V_1}\right|_{I_2=0} = \frac{\Delta}{j\omega(L_{k1}+L_m) - j\omega^3(L_{k1}L_{k2}+L_mL_{k2}+L_m\frac{L_{k1}}{n^2})\ (C_2+C_3)} \qquad (5)$$

Short-circuit admittance on the high-voltage side (Figure 75)

$$\left.\frac{I_1}{V_1}\right|_{V_2=0} = \frac{1-\omega^2\ L_{KP}(C_1+C_3)}{j\omega L_{KP}} \qquad (6)$$

Where $L_{KP} = \frac{L_{K1}L_{K2} + L_m(L_{K2}+L_{K1}/n^2)}{L_{K2} + L_m/n^2}$ is the short-circuit inductance as measured on the high-voltage side for low frequencies.

No-load admittance on the low-voltage side (Figure 76)

$$\left.\frac{I_2}{V_2}\right|_{I_1=0} = \frac{\Delta}{j\omega(L_{k2}+\frac{L_m}{n^2}) - j\omega^3(L_{k1}L_{k2}+L_mL_{k2}+L_m\frac{L_{k1}}{n^2})(C_1+C_3)} \tag{7}$$

Short circuit admittance on the low-voltage side (Figure 77)

$$\left.\frac{I_2}{V_2}\right|_{V_1=0} = \frac{1-\omega^2L_{KS}(C_2+C_3)}{j\omega L_{KS}} \tag{8}$$

where $L_{KS} = \dfrac{L_{K1}L_{K2} + L_m(L_{K2}+L_{K1}/_{n^2})}{L_{K1}+L_m}$ is the short-cicuit inductance as measured on low-voltage side for low frequencies.

Transfer from the high-voltage to the low-voltage side (Figure 78).

$$\left.\frac{V_2}{V_1}\right|_{I_2=0} = \frac{\frac{L_m}{n} - \omega^2\ (L_{k1}\ L_{k2} + L_m\ L_{k2} + L_m\ \frac{L_{k1}}{n^2})\ C_3}{L_{k1} + L_m - \omega^2\ (L_{k1}\ L_{k2} + L_m\ L_{k2} + L_m\ \frac{L_{k1}}{n^2})\ (C_2 + C_3)} \tag{9}$$

Transfer from the low-voltage to the high-voltage side (Figure 79)

$$\left.\frac{V_1}{V_2}\right|_{I_1=0} = \frac{\frac{L_m}{n} - \omega^2(L_{k1}\ L_{k2} + L_m\ L_{k2} + L_m\ \frac{L_{k1}}{n^2})\ C_3}{L_{k2} + \frac{L_m}{n^2} - \omega^2(L_{k1}\ L_{k2} + L_m\ \frac{L_{k1}}{n^2} + L_mL_{K2})(C_1+C_3)} \tag{10}$$

Normally, the iron inductance L_m is much higher than the leakage inductances L_{K1} and n^2L_{K2}, especially for low frequencies . This gives the well known form for the short-circuit inductances.

$$L_{KP} = L_{K1} + n^2L_{K2} \tag{11}$$

$$L_{KS} = L_{K2} + L_{K1}/_{n^2} \tag{12}$$

From the expressions (5) through (10) resonant frequencies can be derived. Assuming $L_m >> L_{K1}$, $L_m >> n^2 L_{K2}$ and $n^2 >> 1$ the next frequencies can be found.

$$f_1 = \frac{1}{2\pi\sqrt{(L_{K2}+\frac{1}{n^2} L_{K1})(C_2+C_3)}} \qquad (13)$$

At this frequency there's a maximum transfer h.v. to l.v., a maximum no-load admittance h.v. and a minimum short-circuit admittance l.v..

$$f_2 = \frac{1}{2\pi\sqrt{L_m (C_1+C_3)}} \qquad (14)$$

At this frequency there are minimum no-load admittances h.v. as well as l.v.

$$f_3 = \frac{1}{2\pi\sqrt{(L_{K1}+n^2 L_{K2})(C_1+C_3)}} \qquad (15)$$

A minimum short-circuit admittance h.v., a maximum no-load admittance l.v., and a maximum transfer l.v. to h.v.

$$f_4 = \frac{1}{2\pi\sqrt{(\frac{L_{K1}}{n} + n\, L_{K2})C_3}} \qquad (16)$$

Here is a minimum transfer h.v. to l.v. as well as l.v. to h.v. When the turns-ratio becomes negative, as was in case of the measured transformer, this resonance disappears.

$$f_5 = \frac{1}{2\pi\sqrt{(\frac{L_{K1}}{n^2} + L_{K2})\ (C_2 + \frac{C_1 C_3}{C_1+C_3})}} \qquad (17)$$

Minimum no-load admittance h.v. and l.v.

This model will be checked using the measurements on the center leg. Here the next frequencies were found.

f_1 = 64 kHz ± 400 Hz
f_2 = 700 Hz ± 300 Hz
f_3 = 10 kHz ± 2 kHz
f_5 = 68 kHz ± 1 kHz

Because f_1 and f_5 almost coincide the no-load admittance h.v. does not show a pronounced maximum at f_1 nor a minimum at f_5.

Resonances on high-voltage side can't be situated accurately because of part-winding resonances. But the capacitances can be determined directly from the high-frequency behaviour. The no-load capacitance on the high-voltage side is given by

$$C_{NP} = \left[j\omega \frac{V_1}{I_1} \bigg|_{\substack{I_2=0 \\ \omega \to \infty}} \right]^{-1} = C_1 + \frac{C_2 C_3}{C_2 + C_3} \qquad (18)$$

The short-circuit capacitance on the high-voltage side has been given by

$$C_{SP} = \left[j\omega \frac{V_1}{I_1} \bigg|_{\substack{V_2=0 \\ \omega \to \infty}} \right]^{-1} = C_1 + C_3 \qquad (19)$$

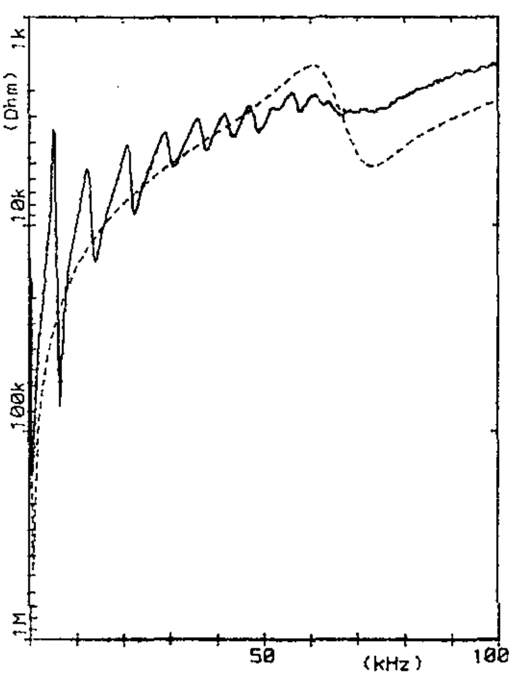

Figure 74: No-load h.v.

Measurements give the following results.

C_{NP} = 770 ± 20 pF

C_{SP} = 850 ± 20 pF

From these values and the values of f_1 and f_8 together with the measured value of the short-circuit inductance approximations for the capacitances in figure 73 can be made.

C_1+C_3 = 850 ± 20 pF

C_2+C_3 = 1950 ± 20 pF

C_3 = 400 ± 100 pF

C_1 = 450 ± 100 pF

C_2 = 1550 ± 100 pF

The uncertanties are mainly caused by the uncertainty in capacitance between high-voltage and low-voltage windings. Because of the negative turns-ratio of this transformer there is no resonance only caused by C_3.

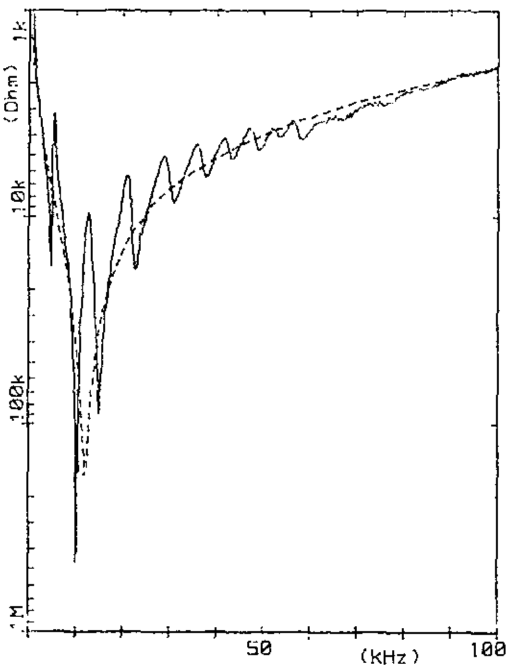

Figure 75: Short-circuit h.v.

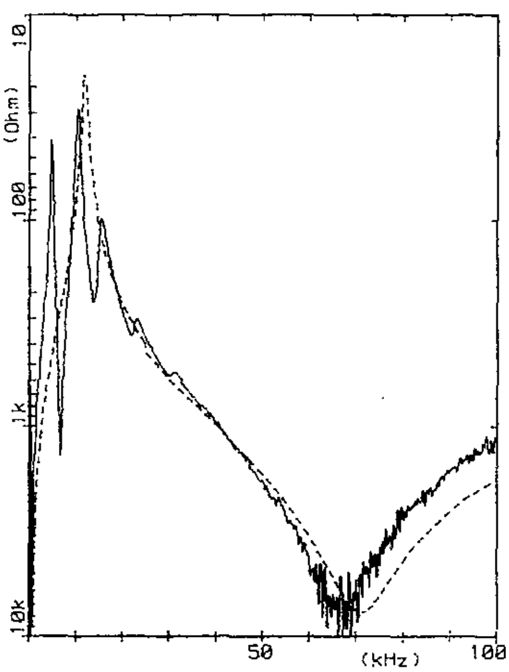

Figure 76: No-load l.v.

One of the main problems in modelling the transformer is the value of the resistors. In this case two sets of values are used. In the frequency region up to 25 kHz the values valid for 10 kHz are applied.

$R_{K1} = 600\ \Omega$, $R_{K2} = 10\ \Omega$.

They are determined from the short-circuit admittance on low-voltage side. Above 25 kHz the values valid for 60 kHz are used

$R_{K1} = 6000\ \Omega$ $R_{K2} = 100\ \Omega$

They are also determined from the short-circuit admittance on low-voltage side. (figure 41) under the assumption that the resistance is equally distributed over the h.v. and the l.v. windings.

Other values used in the one-phase model were

$L_{K1} = 100$ mH

$L_{K2} = 1.6$ mH

(The measured leakage inductance of 200 mH on h.v. side is supposed to be equally distributed over both windings.)

$n = -7.9$

$L_m = 30$ H

(This value has been measured with low-voltage stationairy frequencies of a few hundreds of Hz.)

$R_m = 500$ kΩ

(Determined from the value of the first minimum of the no-load h.v.)

$C_1 = 450$ pF

$C_2 = 1550$ pF

$C_3 = 400$ pF

By using this model admittances and voltage transfers were derived and compared with the measurements on the center leg shown in chapter 3. The results are given in the figures 74 through 79. The dotted curves are model results, The solid curves are measurements.

The jump in some of the dotted curves at 25 kHz is caused by the transition between both models.

Great simularity can be seen between model and measurements. The fast repetition of minima and maxima cannot be explained by this simple model, but the more general properties can. At 10 kHz the model damping seems to agree with measurements, but at 60 kHz the model damping is too low at the high-voltage side. A more complex model is needed to explain all the characteristics. In chapter 4.3 some suggestions are given.

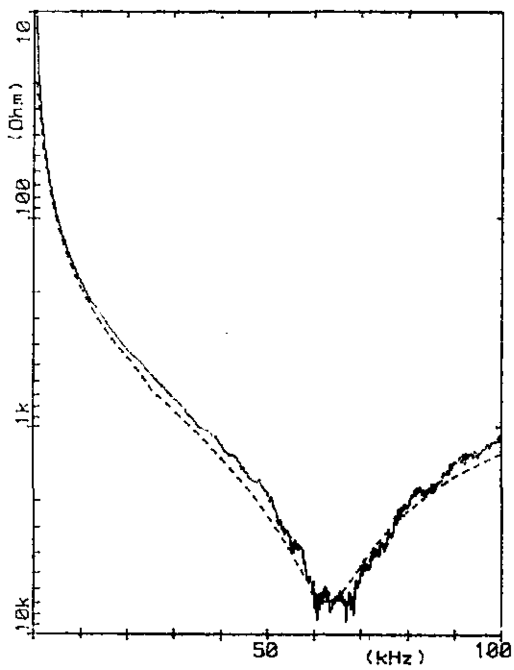

Figure 77: Short-circuit l.v.

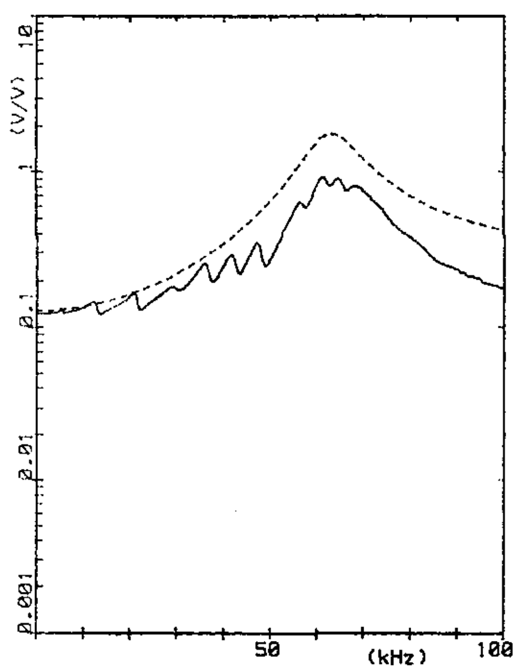

Figure 78: Transfer h.v. to l.v.

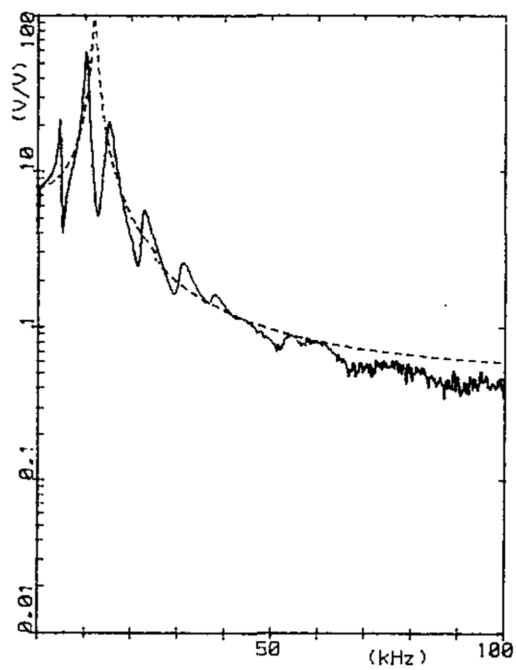

Figure 79: Transfer l.v. to h.v.

4.2 Three-phase model.

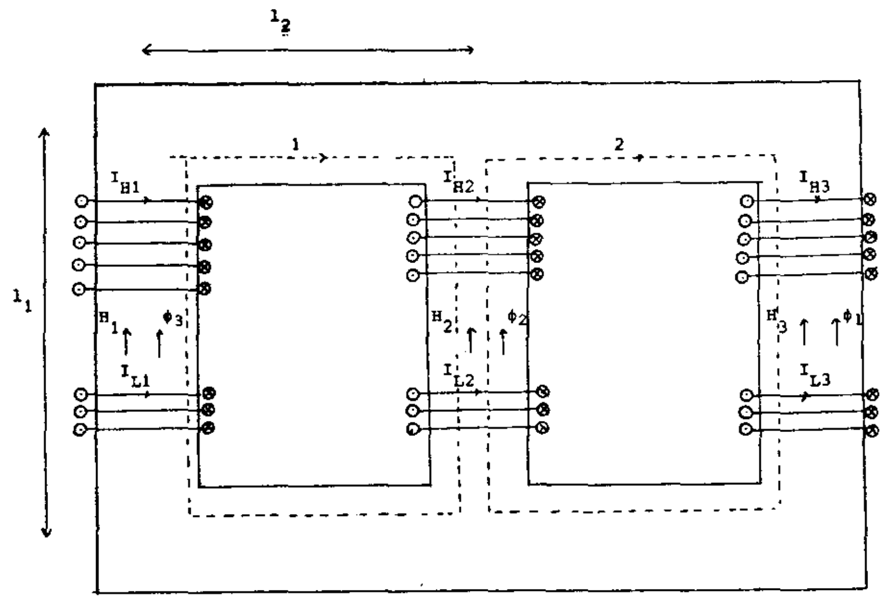

In this chapter a simple transformer model has been used to explaine the difference between the center leg and the outside legs in the frequency-range up to 1 kHz. Figure 80 gives the magnetic part of the transformer.

Figure 80: Simple three-phase transformer model

Using amperes law for path 1 and path 2 gives

$$H_1(l_1 + 2l_2) - H_2 l_1 = N_H I_{H1} + N_L I_{L1} - N_H I_{H2} - N_L I_{L2} \qquad (18)$$

$$H_2 l_1 - H_3(l_1 + 2l_2) = N_H I_{H2} + N_L I_{L2} - N_H I_{H3} - N_L I_{L3} \qquad (19)$$

Where

N_H is the number of turns for the high-voltage winding;

N_L is the number of turns for the low-voltage winding.

The voltage across the windings is determined by flux variations

$$V_{H1} = j\omega N_H \Phi_1 \qquad (3)$$

$$V_{H2} = j\omega N_H \Phi_2 \qquad (4)$$

$$V_{H3} = j\omega N_H \Phi_3 \qquad (5)$$

$$V_{L1} = j\omega N_L \Phi_1 \qquad (6)$$

$$V_{L2} = j\omega N_L \Phi_2 \qquad (7)$$

$$V_{L3} = j\omega N_L \Phi_3 \qquad (8)$$

Flux conservation (Gauss' law) gives

$$\Phi_1 + \Phi_2 + \Phi_3 = 0 \qquad (9)$$

The approximations made uptill now are:

- no leakage flux, so all flux generated by the windings remains in the magnetic material;
- in one leg there's only one flux, so flux variations in one part of the leg follow flux variations in another part immediately.

Leakage flux can be incorporated quite easy, but the number of equations in that case makes an easy analytic interpretation very difficult. For higher frequencies leakage fluxes can't be neglected compared to iron-fluxes because of eddy currents limiting the latter.
Supposing there's just one relative permeability μ_r for the whole iron-core gives the following relations between flux and magnetic fieldstrength.

$$\phi_1 = A\ \mu_0\mu_r\ H_1 \qquad (10)$$

$$\phi_2 = A\ \mu_0\mu_r\ H_2 \qquad (11)$$

$$\phi_3 = A\ \mu_0\mu_r\ H_3 \qquad (12)$$

In this case hysteresis effects and flux-dependence of μ_r are neglected.All non-linear effects must be described by the equations (10) through (12)

Combining (1) through (12) gives a set of equations for winding voltage and winding current. Hereby $X_0 = \mu_0\mu_r N_H A$

$$V_{H1}(l_1+2l_2) - V_{H2}l_1 = j\omega X_0(\ N_H I_{H1} + N_L I_{L1} - N_H I_{H2} - N_L I_{L2}) \qquad (13)$$

$$V_{H2}l_1 - V_{H3}(l_1+2l_2) = j\omega X_0(\ N_H I_{H2} + N_L I_{L2} - N_H I_{H3} - N_L I_{L3}) \qquad (14)$$

$$V_{H1} + V_{H2} + V_{H3} = 0 \qquad (15)$$

$$N_H V_{L1} = N_L V_{H1} \qquad (16)$$

$$N_H V_{L2} = N_L V_{H2} \qquad (17)$$

$$N_H V_{L3} = N_L V_{H3} \qquad (18)$$

These equations describe the behaviour of a three-phase transformer. Other network elements, like capacitances, can be added to this model.
Connecting a capacitor C parallel to the high-voltage winding, while leaving the low-voltage winding in no-load, gives the following equations for transfer from leg 1 to leg 2 and leg 3.

$$\frac{V_{H2}}{V_{H1}} = -\frac{l_1+2l_2 - \omega^2 C X_0 N_H}{2l_1+2l_2 - 2\omega^2 C X_0 N_H} \qquad (19)$$

$$\frac{V_{H3}}{V_{H1}} = -\frac{l_1 - \omega^2 C X_0 N_H}{2l_1+2l_2 - 2\omega^2 C X_0 N_H} \qquad (20)$$

The no-load admittance of the high-voltage winding on the outside leg is given by:

$$Y = j\omega C + \frac{1}{j\omega X_0 N_H}\left[l_1+2l_2+(l_1-\omega^2 C X_0 N_H)\frac{l_1+2l_2- \omega^2 C X_0 N_H}{2l_1+2l_2-2\omega^2 C X_0 N_H}\right] \qquad (21)$$

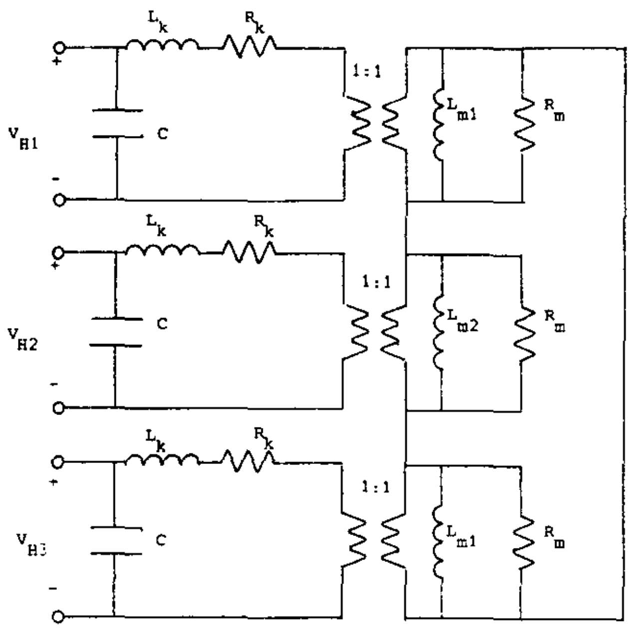

Figure 81: *3-phase network model*

The model used in this chapter can be translated to the network-model shown in figure 81. Only high-voltage windings are shown, the short-circuit impedance $R_K+j\omega L_K$, the magnetization resistance R_m and the capacitance of the high-voltage winding in no-load C have been added to the model of figure 80.

L_{m1} and L_{m2} are related to the earlier model as

$$L_{m1} = \frac{\mu_0\mu_r N_H^2 A}{l_1+2l_2}$$

$$L_{m2} = \frac{\mu_0\mu_r N_H^2 A}{l_1}$$

The next quantities have been used in the network model.

$L_K = 200$ mH
$R_K = 50\ \Omega$

(Inductance and resistance determined from short-circuit l.v.S at about 1000 Hz.)

C = 770 pF

(capacitance measured in no-load on h.v. side for high frequencies.)

$L_{m1} = 50$ H
$L_{m2} = 140$ H

(Values determined from low-voltage measurements of no-load induction for the three legs on h.v. side at stationairy frequencies)

$R_m = 1.5$ MΩ

(Determined by trial-and-error to reproduce the double peak in figure 83.)

This gives the results shown in figures 82 through 84.

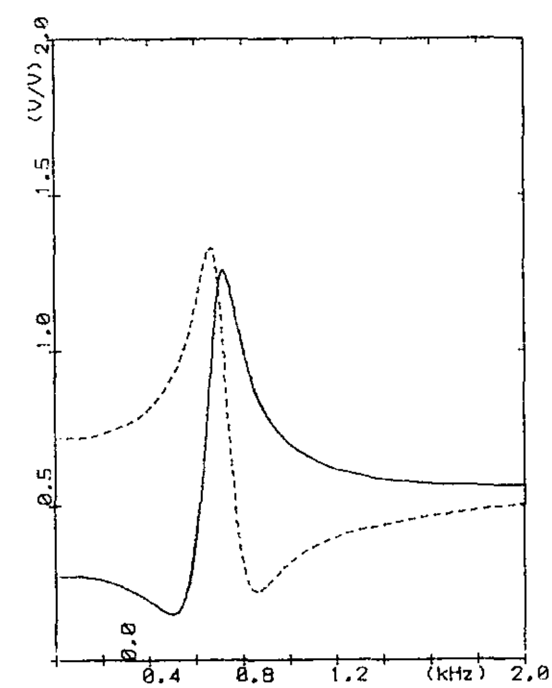

Figure 82: *transfer from outside leg to other legs*

Figure 82 shows the transfer from the high-voltage side of an outside leg to the high-voltage side of the center leg (dotted curve) and to the other outside leg (solid curve). They must be compared with the measurements as shown in figure 63 in chapter 3. The no-load impedances have been given in figures 83 (outside leg) and 84 (center leg), they must be compared to figure 19 and 50 of chapter 3 respectively.
It is shown here that the characteristics of impedance and transfer can be reproduced fairly well.

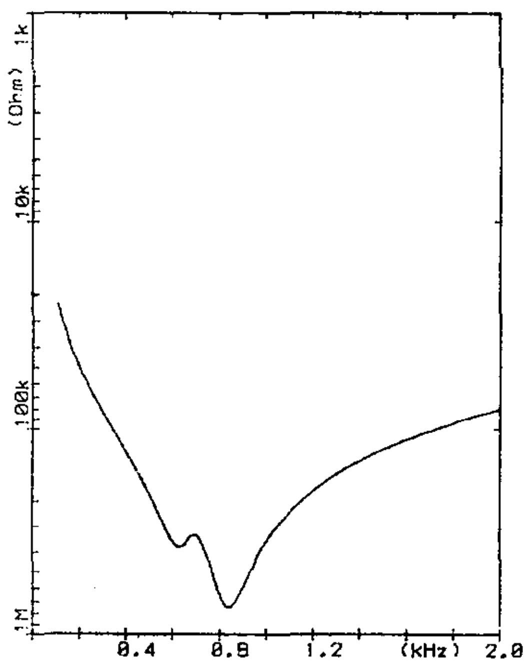

Figure 83: No-load h.v. outside leg

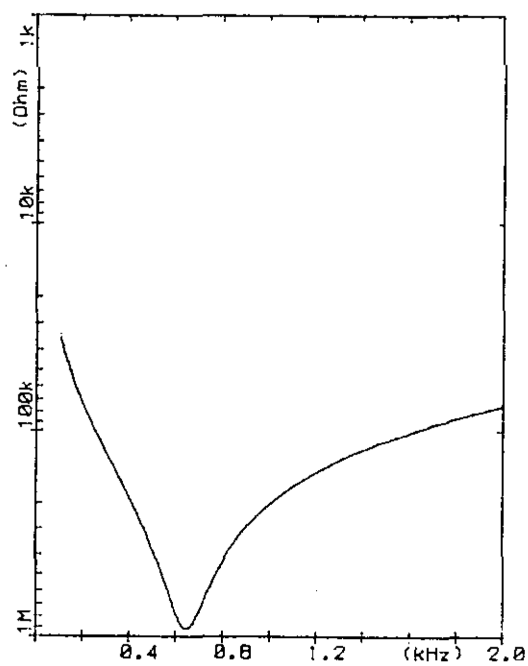

Figure 84: No-load h.v. center leg

4.3 Conclusions and future work.

In chapter 4.1 a single-phase model is applied to explain the behaviour of high- and low-voltage windings on the center leg. It is possible to reproduce the large scale behaviour from the low-frequency parameters (no-load and short-circuit impedance and turns-ratio) and three capacitances. The capacitance of the high-voltage winding to earth can be determined from the high-frequency behaviour of no-load and short-circuit impedance, which is almost pure capacitive. The capacitance of the low-voltage winding to earth has been determined from the resonant frequency of short-circuit inductance and capacitance. On high-voltage side these frequencies are hidden by part-winding resonances. The capacitance between high-voltage winding and low-voltage winding has been determined from the differences in no-load and short-circuit capacitance.

The major problem is the choice of the resistances. The resistance representing the copper losses varies from a few ohm at 50 Hz to tens of kΩ at 100 kHz (transformed to low-voltage side). By using a stepwise variation of the resistance at 25 kHz a fairly good representation is possible. Some abberations are seen on high-voltage side near 65 kHz.

Frequency dependence of no-load inductance and of the resistance responsible for the iron losses have not been taken into account. Because all effects of these latter two are at low frequencies (below a few kHz) this frequency dependence is probably not very important for the model given here.

The part-winding resonances (visible up to 70 kHz) can not be explained by the simple model used.

In chapter 4.2 a three-phase model has been used to explain the low-frequency behaviour of no-load admittances of high-voltage windings and the transfer between the windings of different legs. (up to 2 kHz). No-load and short-circuit inductance (measured at 50 Hz) were applied, together with the "total capacitance" of the high-voltage winding to earth in no-load. The transfer from an outside leg to the other legs can be reproduced, as well as both no-load admittances. Problems arise in explaining the transfer from the center leg to the outside legs. According to the model the transfer is independent of frequency, but according to measurements there's a mimimal transfer to both outside legs at 750 Hz (the resonant frequency of the outside legs). This is probably caused by fluxes through air when the outside legs are in resonance. In the model used these fluxes are neglected.

To reproduce all measurements a more sophisticated model is needed, including both models used here. Each winding must be divided in segments to represent part winding resonances. Also air fluxes should be included in the model. The inductance of each segment consists of an iron part and a leakage part. Because every segment carries the same flux, the voltages accross all iron parts are equal. For the transfer to windings on other legs the frequency dependence of the iron inductance is probably very important. At the moment no measurements are carried out for the iron inductances as a function of frequency over a large frequency range.

The leakage impedance as a function of frequency can be derived from the short-circuit impedance of the low-voltage winding. The inductance is frequency independent, but the resistance is not at all. This frequency dependence should be included in a future model.

More future measurements are needed on non-linear effects because of the flux-dependence of iron characteristics. Non-lineair effects have been already determined at no-load impedance of the outside leg. No non-linear effects are found at the no-load impedance of the center leg, but use of higher voltages will surely show them. Also non-linear effects are expected in the transfer between windings on different legs.

Last but not least more transformers are needed to see if the simple models presented in this work hold for all transformers.

5. Conclusions.

In the preceeding chapters a number of frequency spectra of admittances and voltage transfers measured on a power transformer have been given. They are derived by Fourier transform of the input voltage and the input current and output voltage respectively. By comparison between these results and results obtained with a sweep generator the method has been shown to be reliable. Phenomena between 1 kHz and some hundreds of kHz can be reproduced in most cases. Problems arise when using this method for phenomena below 1 kHz. The 2k words storage buffer of the digitizer does not give enough frequency resolution to reproduce these phenomena. With the chosen sample frequency a larger storage buffer (10 - 20k words) will be needed to reproduce the low frequency phenomena with the pulse method. In this work measurements with a sweep generator and with stationairy frequencies have been used to show the low frequency phenomena.
Problems also arise in frequency ranges where one of the two signals has a low energy content. A high noise level occurs in these frequency ranges. This is most clearly visible with the transfer from a low-voltage side to the high-voltage side on another leg, giving a high low-frequency transfer and a low high-frequency transfer. The high noise level appears above 50 kHz (see for example figure 46). A higher bit resolution (12 or 14 bit in stead of 10 bit) is needed to show the high-frequency transfer in this case.

The measurements of single-phase phenomena like input admittances and transfer to the other side of the same leg show a large scale behaviour explained by a simple model. This model consists of the low-frequency parameters (no-load and short-circuit impedance at 50 Hz, and the turns ratio) together with three capacitances. The capacitances on high-voltage side are derived from the high-frequency behaviour, the capacitances on low-voltage side are derived from resonant frequencies. The same model is used by Glaninger(1983) to get expressions for the no-load impedance as a function of frequency. Models for transformers with more windings using only capacitance and inductance for a complete winding have been used by Degeneff et. al.(1982) and Adielson et.al.(1981). They compare measured impedances and transfers with model results. Both show good agreement for the large scale behaviour up to some tens of kHz.

Superimposed on this large scale behaviour are maxima and minima , probably caused by part winding resonances of the leakage flux. The maxima in the input admittance are the same in no-load and in short-circuit situation. The frequencies on low-voltage side are slightly lower than those on high-voltage side. The outside legs show extra resonances compared to the center leg. The frequencies visible in the input admittance return in the transfer to the other side as well as in the transfer to other legs. The measurements of Adielson et. al.(1981) also show minima and maxima superimposed on a large scale behaviour explained by their model. The frequencies in the impedance return in the transfer to the same leg. Transfers to other legs have not been shown.

From the short-circuit admittance on low-voltage side, inductance and resistance can be derived. The inductance (leakage inductance) has been shown to be frequency independent up to 100 kHz. The resistance (copper loss) shows a steady increase with increasing frequency.

By dividing the transfer to the high-voltage side by the transfer to the low-voltage side (both on the same leg) the flux linkage between high-voltage side and low-voltage side has been made visible. Up to 30 kHz both windings enclose the same flux. For higher frequencies flux linkage is no longer present. The iron flux seems to dominate over the leakage flux up to 30 kHz.

The transfer from one leg to another can be divided into four groups. The transfer from high-voltage to high-voltage side shows a low-frequency value of 0.5 V/V followed by a slow but steady decrease. The high-frequency value (capacitive transfer) of about 0.1 V/V is reached above 100 kHz. The transfer from high-voltage to low-voltage side shows a low-frequency value of 0.06 V/V followed by a slow decrease up to a minimum around 45 kHz. Around 65 kHz there is a broad maximum. After that the transfer decreases to reach the high-frequency value of about 0.01 V/V around 150 kHz. The transfer from low-voltage to high-voltage side starts with a low-frequency value of 4 V/V followed by a maximum around 10 kHz. For higher frequencies it shows a fast decrease up to 50 kHz, where the behaviour is lost in the noise. The transfer from low-voltage to low-voltage side shows a low-frequency value of 0.5 V/V, a maximum around 10 kHz, a minimum around 45 kHz and a maximum around 65 kHz. All transfers show maxima and minima superimposed on this large scale behaviour.

The difference between the center leg and the outside legs in the frequency range up to 1 kHz has been explained by a three-phase model consisting mainly of flux paths in the core of the transformer. The leakage impedance and the capacitance of the high-voltage winding to earth have been added to the model. The no-load admittances and the transfer to the other legs have been reproduced by this model.

Non-linear effects are shown in the no-load admittances on high-voltage side and are suspected in the no-load admittance on low-voltage side and the transfer from one leg to another. These non-linear effects are limited to noload situations and to the frequency range below 1 kHz. They can be important for modelling purposes but have no effect on transformer testing with the pulse response method.

References

Adielson, T. and Å. Carlson, H.B. Margolis, J.A. Halladay
RESONANT OVERVOLTAGES IN EHV TRANSFORMERS: Modeling and application.
IEEE Trans. Power Appar. & Syst., Vol. PAS-100(1981), p. 3563-3572.

Dick, E.P. and C.C. Erven
TRANSFORMER DIAGNOSTIC TESTING BY FREQUENCY RESPONSE ANALYSIS.
IEEE Trans. Power Appar. & Syst., Vol. PAS-97(1978), p. 2144-2153.

Degeneff, R.C. and W.J. McNutt, W. Neugebauer, J. Panek, M.E. McCallum, C.C. Honey
TRANSFORMER RESPONSE TO SYSTEM SWITCHING VOLTAGES.
IEEE Trans. Power Appar. & Syst., Vol. PAS-101(1982), p. 1457-1470.

Glaninger, P.
DAS SCHWINGUNGSVERHALTEN EINES EINFACHEN TRANSFORMATOR-ERSATZ-SCHALTBILDES.
etzArchiv, Vol. 5(1983), p. 369-375.

Roth, P.R.
EFFECTIVE MEASUREMENTS USING DIGITAL SIGNAL ANALYSIS.
IEEE Spectrum, Vol. 8, No. 4(April 1971), p. 62-70.

Vaessen, P.T.M.
TRANSFORMER MODEL FOR HIGH FREQUENCIES.
IEEE/PES Summer Meeting, San Francisco, Cal., 12-17 July 1987.
Paper No. 87SM538-2.

Wagner, K.W.
DAS EINDRINGEN EINER ELEKTROMAGNETISCHEN WELLE IN EINE SPULE MIT WIRKUNGSKAPAZITÄT.
Elektrotech. & Maschinenbau (EuM), Vol. 33(1915), p. 89-95.

Appendix A. Transformer data.

Manufacturer: Smit transformers B.V. Nijmegen, Netherlands.

Type: 25 MVA, 150/11 kV, Yd 5

Core:	type	: Three leg core
	window height	: 2250 mm
	window width	: 570 mm
	leg diameter	: 735 mm
	leg crossection	: 3350 cm^2

Low-voltage winding :	number of turns	: 109
	height	: 1806 mm
	inside diameter	: 785 mm
	outside diameter	: 863 mm

High-voltage winding:	number of turns	: 860
	height	: 1780 mm
	inside diameter	: 1055 mm
	outside diameter	: 1188 mm

An earthed screen is constructed around the low-voltage winding at a diameter of 885 mm. It consists of aluminum strips 0.03 mm thick and 120 mm wide, connected on one side.

Short-circuit impedance on high-voltage side (calculated for 50 Hz)

$X = 60.8\ \Omega$ (194 mH)

$R = 2.74\ \Omega$

$\varepsilon = 6.77\ \%$

No-load impedance on low-voltage side (50 Hz)

$V_{eff} = 10$ kV	$\lvert Z \rvert = 470\ \Omega$	$L = 1500$ mH
$V_{eff} = 11$ kV	$\lvert Z \rvert = 280\ \Omega$	$L = 900$ mH
$V_{eff} = 12$ kV	$\lvert Z \rvert = 170\ \Omega$	$L = 540$ mH

Appendix B: Phase-to-phase measurements.

The figures B1 through B6 give the absolute value of the transfers from one leg to another. The transfers from one winding to the windings on another leg are in the same figure. The solid line is the transfer to the high-voltage winding, the dotted line the transfer to the low-voltage winding.

Figure B1 gives the transfer h.v.S to h.v.R (solid line)
and the transfer h.v.S to l.v.R (dotted line).

Figure B2 gives the transfer h.v.R to h.v.S (solid line)
and the transfer h.v.R to l.v.S (dotted line).

Figure B3 gives the transfer h.v.R to h.v.T (solid line)
and the transfer h.v.R to l.v.T (dotted line).

Figure B4 gives the transfer l.v.S to h.v.T (solid line)
and the transfer l.v.S to l.v.T (dotted line).

Figure B5 gives the transfer l.v.R to h.v.S (solid line)
and the transfer l.v.R to l.v.S (dotted line).

Figure B6 gives the transfer l.v.T to h.v.R (solid line)
and the transfer l.v.R to l.v.T (dotted line).

Outside leg to center leg

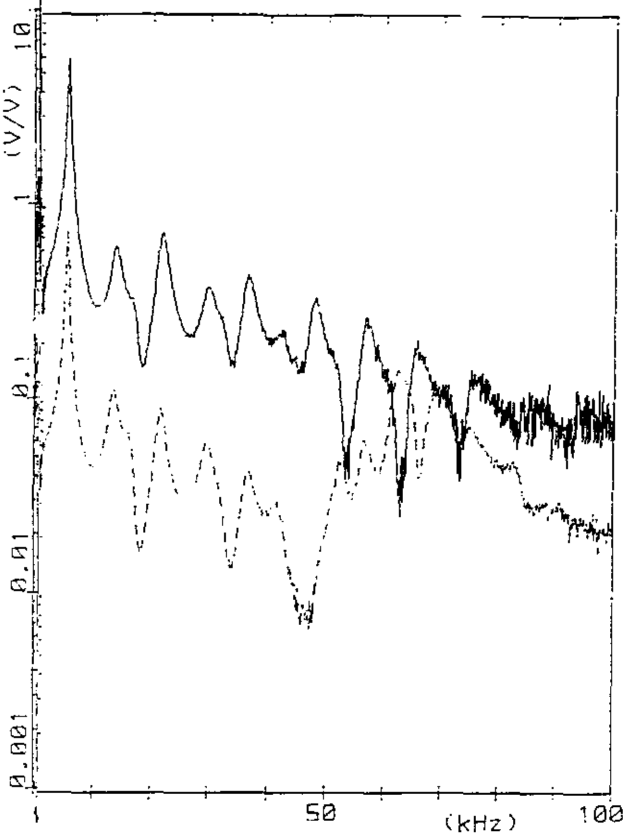

Figure B2 Transfer from h.v.winding

Outside leg to outside leg

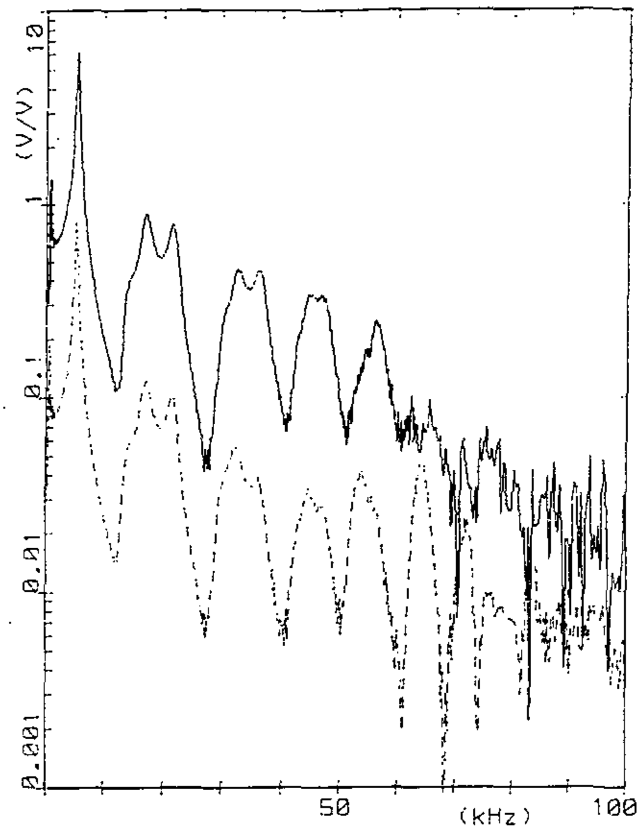

Figure B3 Transfer from h.v. winding

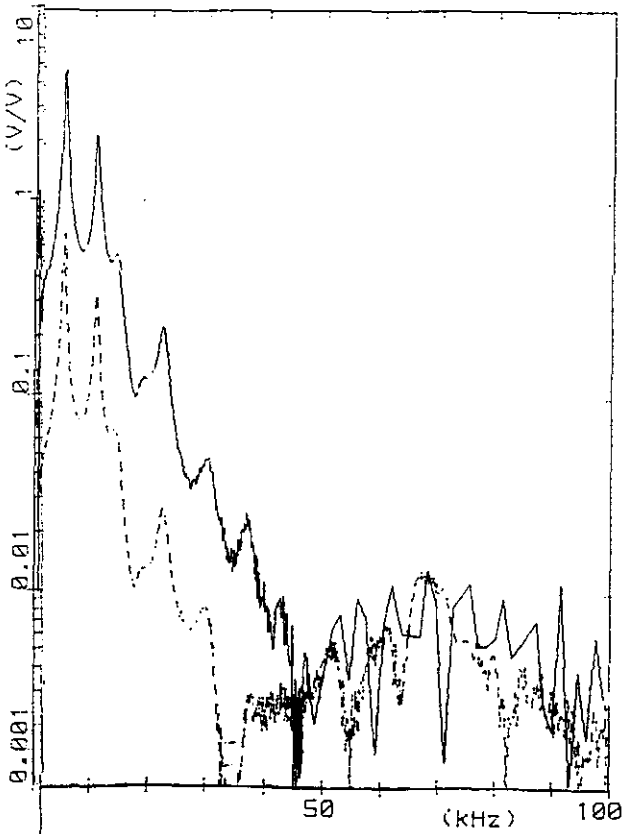

Figure B5 Transfer from l.v. winding

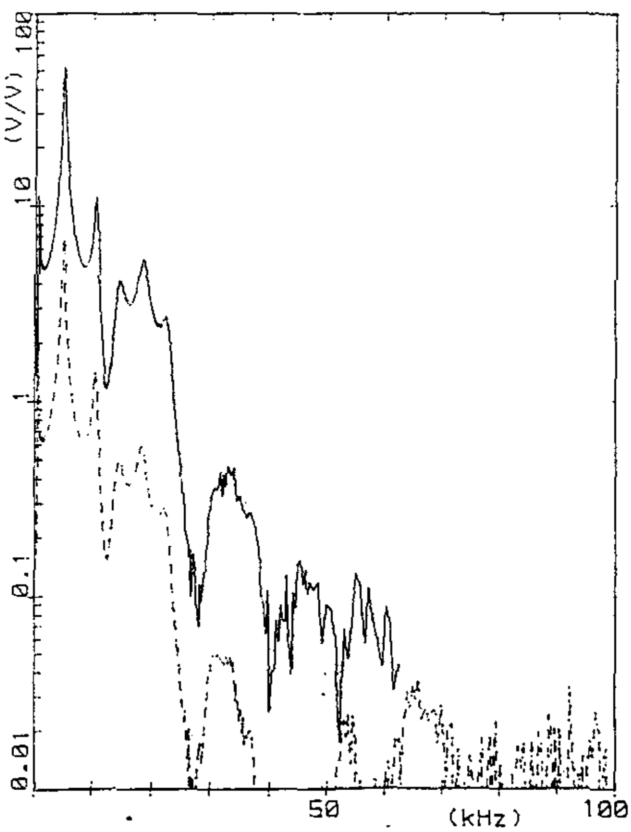

Figure B6 Transfer from l.v. winding

Center leg to outside leg

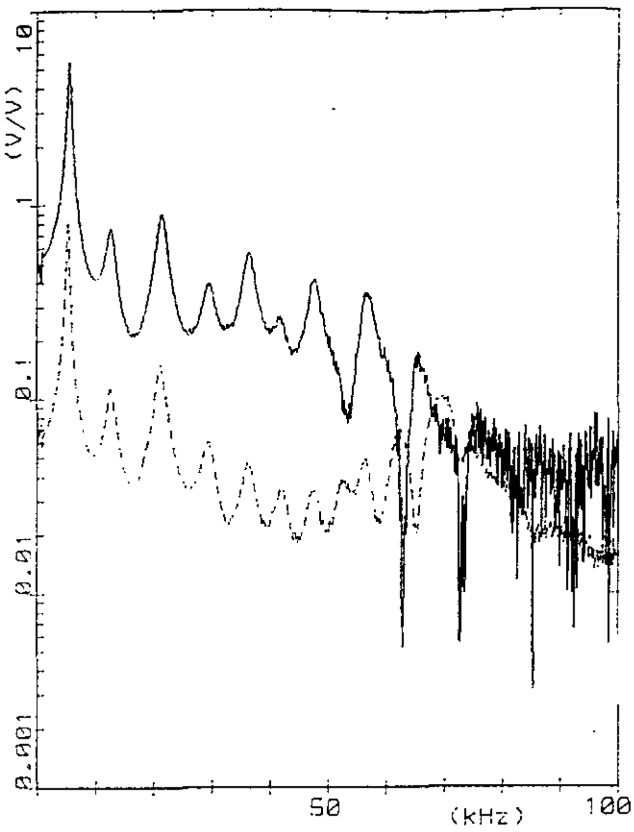

Figure B1 Transfer from h.v.winding

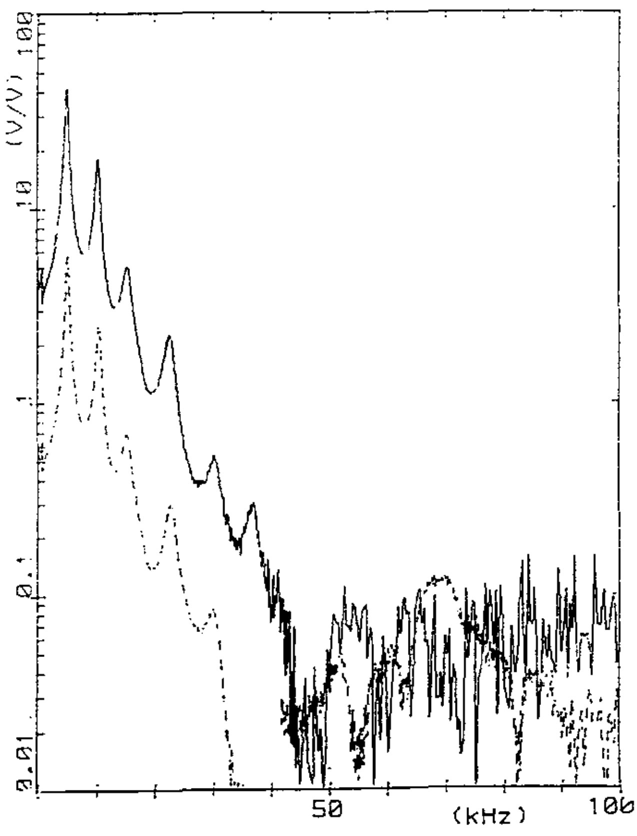

Figure B4 Transfer from l.v. winding

Appendix C: Single-phase measurements.

The figures C1 through C6 give the results of the measurements concerning only one single phase. The solid lines are for the center leg, the dotted lines for an outside leg.

Figure C1 gives the no-load h.v.S and the no-load h.v.T.
Figure C2 gives the short-circuit h.v.S and the short-circuit h.v.T.
Figure C3 gives the no-load l.v.S and the no-load l.v.T.
Figure C4 gives the short-circuit l.v.S.
Figure C5 gives the transfer h.v.S to l.v.S and the transfer h.v.T to l.v.T.
Figure C6 gives the transfer l.v.S to h.v.S and the transfer l.v.T to h.v.T.

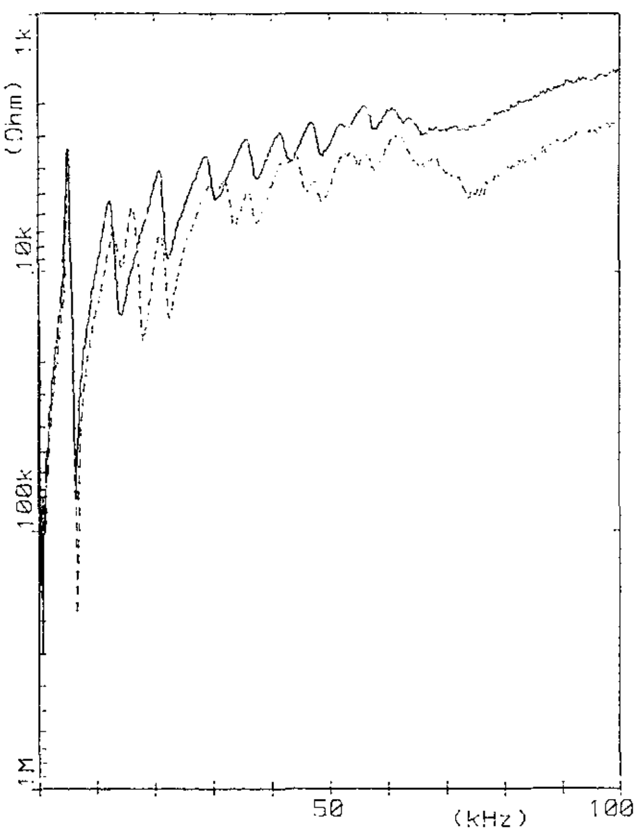

Figure C1: No-load h.v.

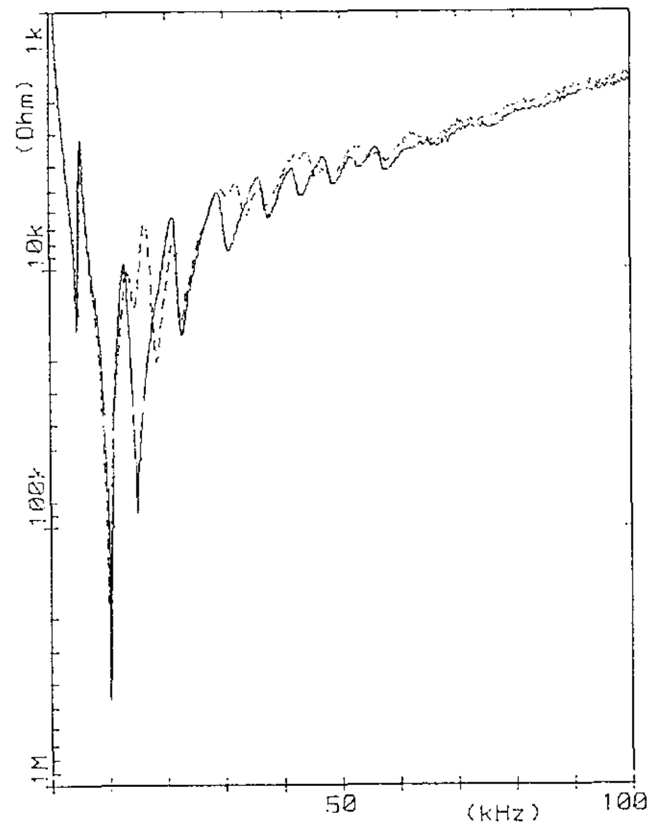

Figure C2: Short-circuit h.v.

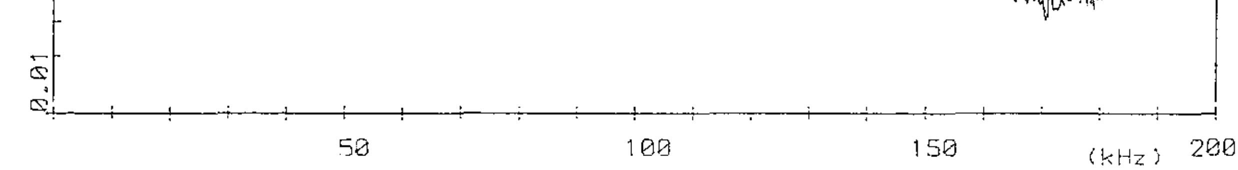

Figure C5: Transfer h.v. to l.v.

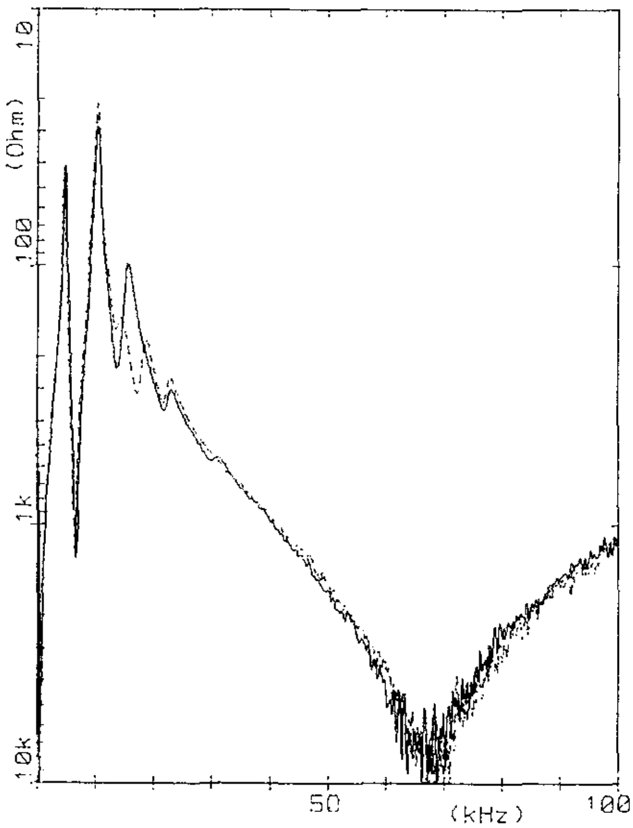

Figure C3: No-load l.v

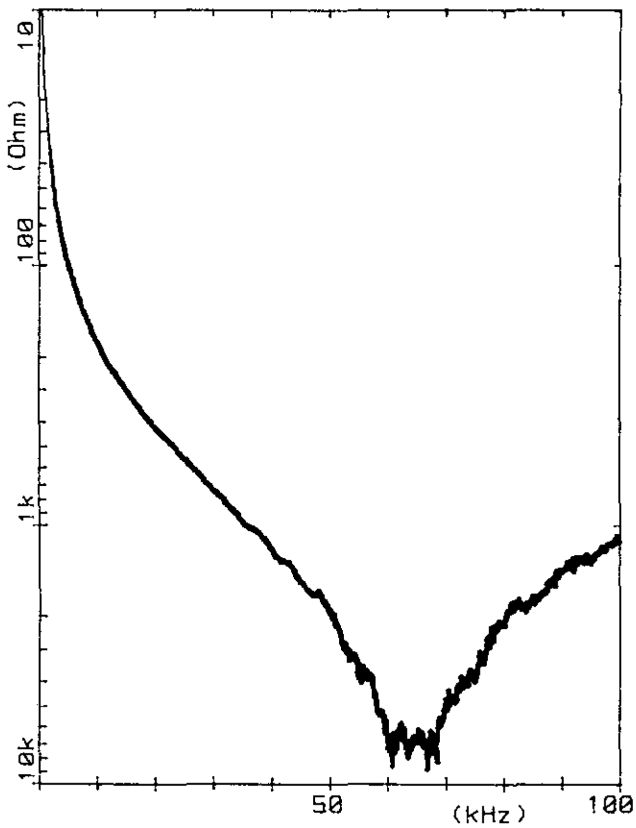

Figure C4: Short-circuit l.v.

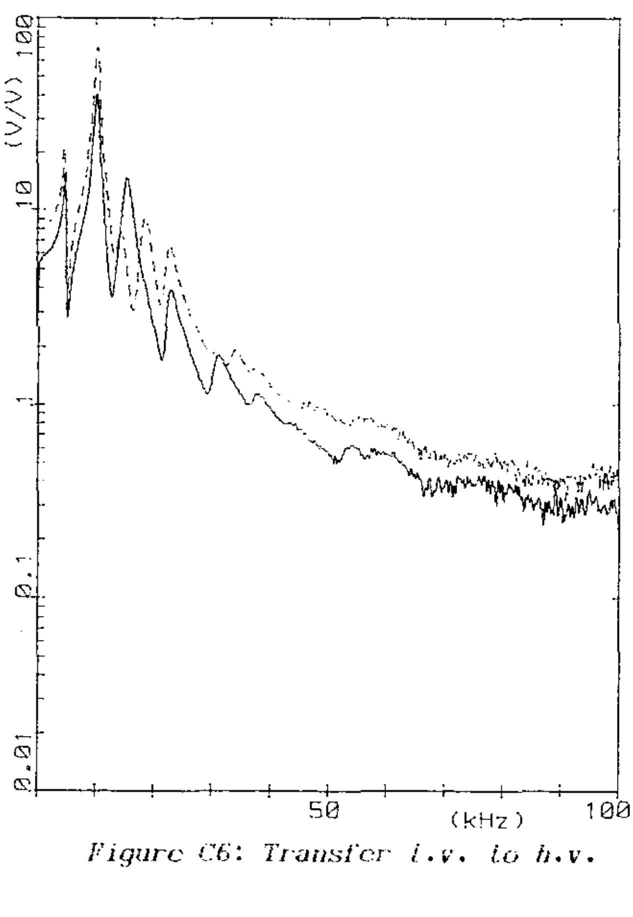

Figure C6: Transfer l.v. to h.v.

ISSN 0167-9708
Coden: TEUEDE

(162) Meer, A.C.P. van
TMS32010 EVALUATION MODULE CONTROLLER.
EUT Report 86-E-162. 1986. ISBN 90-6144-162-5

(163) Stok, L. and R. van den Born, G.L.J.M. Janssen
HIGHER LEVELS OF A SILICON COMPILER.
EUT Report 86-E-163. 1986. ISBN 90-6144-163-3

(164) Engelshoven, R.J. van and J.F.M. Theeuwen
GENERATING LAYOUTS FOR RANDOM LOGIC: Cell generation schemes.
EUT Report 86-E-164. 1986. ISBN 90-6144-164-1

(165) Lippens, P.E.R. and A.G.J. Slenter
GADL: A Gate Array Description Language.
EUT Report 87-E-165. 1987. ISBN 90-6144-165-X

(166) Dielen, M. and J.F.M. Theeuwen
AN OPTIMAL CMOS STRUCTURE FOR THE DESIGN OF A CELL LIBRARY.
EUT Report 87-E-166. 1987. ISBN 90-6144-166-8

(167) Oerlemans, C.A.M. and J.F.M. Theeuwen
ESKISS: A program for optimal state assignment.
EUT Report 87-E-167. 1987. ISBN 90-6144-167-6

(168) Linnartz, J.P.M.G.
SPATIAL DISTRIBUTION OF TRAFFIC IN A CELLULAR MOBILE DATA NETWORK.
EUT Report 87-E-168. 1987. ISBN 90-6144-168-4

(169) Vinck, A.J. and Pineda de Gyvez, K.A. Post
IMPLEMENTATION AND EVALUATION OF A COMBINED TEST-ERROR CORRECTION PROCEDURE FOR MEMORIES WITH DEFECTS.
EUT Report 87-E-169. 1987. ISBN 90-6144-169-2

(170) Hou Yibin
DASM: A tool for decomposition and analysis of sequential machines.
EUT Report 87-E-170. 1987. ISBN 90-6144-170-6

(171) Monnee, P. and M.H.A.J. Herben
MULTIPLE-BEAM GROUNDSTATION REFLECTOR ANTENNA SYSTEM: A preliminary study.
EUT Report 87-E-171. 1987. ISBN 90-6144-171-4

(172) Bastiaans, M.J. and A.H.M. Akkermans
ERROR REDUCTION IN TWO-DIMENSIONAL PULSE-AREA MODULATION, WITH APPLICATION TO COMPUTER-GENERATED TRANSPARENCIES.
EUT Report 87-E-172. 1987. ISBN 90-6144-172-2

(173) Zhu Yu-Cai
ON A BOUND OF THE MODELLING ERRORS OF BLACK-BOX TRANSFER FUNCTION ESTIMATES.
EUT Report 87-E-173. 1987. ISBN 90-6144-173-0

(174) Berkelaar, M.R.C.M. and J.F.M. Theeuwen
TECHNOLOGY MAPPING FROM BOOLEAN EXPRESSIONS TO STANDARD CELLS.
EUT Report 87-E-174. 1987. ISBN 90-6144-174-9

(175) Janssen, P.H.M.
FURTHER RESULTS ON THE McMILLAN DEGREE AND THE KRONECKER INDICES OF ARMA MODELS.
EUT Report 87-E-175. 1987. ISBN 90-6144-175-7

(176) Janssen, P.H.M. and P. Stoica, T. Söderström, P. Eykhoff
MODEL STRUCTURE SELECTION FOR MULTIVARIABLE SYSTEMS BY CROSS-VALIDATION METHODS.
EUT Report 87-E-176. 1987. ISBN 90-6144-176-5

(177) Stefanov, B. and A. Veefkind, L. Zarkova
ARCS IN CESIUM SEEDED NOBLE GASES RESULTING FROM A MAGNETICALLY INDUCED ELECTRIC FIELD.
EUT Report 87-E-177. 1987. ISBN 90-6144-177

(178) Janssen, P.H.M. and P. Stoica
ON THE EXPECTATION OF THE PRODUCT OF FOUR MATRIX-VALUED GAUSSIAN RANDOM VARIABLES.
EUT Report 87-E-178. 1987. ISBN 90-6144-178-1

(179) Lieshout, G.J.P. van and L.P.P.P. van Ginneken
GM: A gate matrix layout generator.
EUT Report 87-E-179. 1987. ISBN 90-6144-179-X

(180) Ginneken, L.P.P.P. van
GRIDLESS ROUTING FOR GENERALIZED CELL ASSEMBLIES: Report and user manual.
EUT Report 87-E-180. 1987. ISBN 90-6144-180-3

(181) Bollen, M.H.J. and P.T.M. Vaessen
FREQUENCY SPECTRA FOR ADMITTANCE AND VOLTAGE TRANSFERS MEASURED ON A THREE-PHASE POWER TRANSFORMER.
EUT Report 87-E-181. 1987. ISBN 90-6144-181-1